universität wien

MASTERARBEIT / MASTER'S THESIS

Titel der Masterarbeit / Title of the Master's Thesis

„Protein adsorption studies on biomimetic silica particles“

verfasst von / submitted by

Johanna Fehl, BSc

angestrebter akademischer Grad / in partial fulfilment of the requirements for the degree of

Master of Science (MSc)

Wien, 2020 / Vienna 2020

Studienkennzahl lt. Studienblatt / degree programme code as it appears on the student record sheet:	UA 066 862
Studienrichtung lt. Studienblatt / degree programme as it appears on the student record sheet:	Masterstudium Chemie
Betreut von / Supervisor:	Univ.-Prof. Dr. Christian Friedrich Wilhelm Becker
Mitbetreut von / Co-Supervisor:	Meder Kamalov, B.Sc. PhD

Table of contents

Acknowledgements

I would especially like to thank Prof. Christian F. W. Becker, for welcoming me as a part of his working group for seven months thus giving me the opportunity to work in this interesting and promising research field. Thanks for being so patient with me.

I am Dr. Meder Kamalov deeply grateful, for his support and kind supervision during the experimental lab work and writing of this thesis. I wish you all the best for your upcoming challenges.

A thank you also goes to Daniela Reichinger, MSc. (the other silica girl) for all the coke breaks and happy hours singing to Disney music, and to Dr. Friedrich Bialas who always helped my keep my motivation and made me smile. Thanks, for becoming my dear friends.

I would like to thank Gerhard Niederacher for his help with protein expression as well as Dr. Stefan Puchegger, for his help with SEM imaging.

Many thanks also to the whole Becker group, for your continuous support and the fun we had during my internship. I will never forget our trip to Wildalpen.

Thanks to my mum and dad, Susanne and Johannes, who always loved and supported me. Thanks for encouraging and telling me, that everything is possible.

Last but not least, thank you, my beloved fiancé Gunnar, for you have been close at my side during this adventure. There are no words to express my gratitude to you, for all the strength you have given me. I love you.

Abstract

Both improving already existing and developing innovative drug carrier methods is of high relevance due to the increasing amounts of newly discovered bioactive substances. Biomimetic silica combines excellent physicochemical stability with low toxicity and mild synthesis conditions which facilitates its use as drug carrier.

In this thesis, we describe the synthesis of silica particles by using freshly hydrolyzed TMOS and condensation of the resulting silicic acid in presence of the silaffin peptide R5. This method offered the opportunity to attach a fluorescent dye to the peptide, that was then encapsulated in silica during its formation reaction. Protein adsorption properties of R5 silica particles were evaluated with the enhanced green fluorescent protein (eGFP) and thioredoxin (TRX). Additionally, alternative silica particles were synthesized using an R5 conjugate with cyanine-5 (Cy5). We observed that eGFP was released under basic conditions (pH 9) and Cy5-R5 under acidic conditions (pH 3). This load/release approach also worked for silica particles concurrently loaded with eGFP and Cy5-R5, resulting in a specific release of one cargo while the other was retained in the particles.

To conclude, the performed experiments have shown that R5 silica particles can be used as multifunctional carriers of molecular cargo that can be released under specific, orthogonal conditions.

Zusammenfassung

Sowohl die Weiterentwicklung von bereits bestehenden als auch die Entwicklung von neuen Methoden für den Transport von Wirkstoffen ist von großer Wichtigkeit, da die Menge an neu entdeckten bioaktiven Substanzen steigt. Biomimetisches Silica vereint eine exzellente physikochemische Stabilität mit geringer Toxizität und milden Synthese Bedingungen, sodass eine Anwendung als Wirkstoff Transporter ermöglicht wird.
In dieser Arbeit beschreiben wir die Synthese von Silica Partikeln, durch Verwendung von frisch hydrolysiertem TMOS und Kondensationsreaktion der resultierenden Kieselsäure in Anwesenheit des Silaffin Peptids R5.
Diese Methode machte es möglich, einen fluoreszierenden Farbstoff an das Peptid R5 zu koppeln, dass im Silica, während dessen Bildung, eingeschlossen wurde. Die Eigenschaften von R5 Silica Partikeln, ein Protein zu adsorbieren, wurden mithilfe des verstärkt grün fluoreszierenden Proteins (eGFP) und Thioredoxin (TRX) beurteilt. Zusätzlich wurden alternative Silica Partikel, unter Verwendung des R5 Konjugats mit Cyanine-5 (Cy5), synthetisiert. Wir haben beobachtet, dass eGFP unter basischen (pH 9) und Cy5-R5 unter sauren (pH 3) Bedingungen wieder freigesetzt werden konnte. Dieser Ansatz zur Ladung und Freisetzung von Cargo Molekülen funktionierte auch für Silica Partikel, die gleichzeitig mit eGFP und Cy5-R5 beladen waren. Hier kam es zu einer spezifischen Freisetzung einer Cargo, während die andere im Partikel verblieb.
Zusammenfassend zeigten die durchgeführten Experimente, dass R5 Silica Partikel als multifunktionelle Transporter von molekularer Fracht dienen können, die unter spezifischen, orthogonalen Bedingungen wieder freigesetzt werden können.

Abbreviations

Aa	Amino acid
ACN	Acetonitrile
APS	Ammonium persulfate
APTES	(3-aminopropyl) triethoxysilane
Arg	L-Arginine
Boc	Tertbutyloxycarbonyl
Cy5	Cyanine-5
Cy5-R5	Cyanine-5-R5
Cys	L-Cysteine
DCM	Dichloromethane
DIPEA	N, N-Diisopropylethylamine
DMF	Dimethylformamide
DOTMA	N-[1-(2,3-dioleyloxy) propyl]-N,N,N-trimethylammonium chloride
DTNP	2,2'-dithiobis(5-nitropyridine)
DTT	Dithiothreitol
EDTA	Ethylenediaminetetraacetic acid
EGFP	Enhanced green fluorescent protein
Eq	Equivalent
Fmoc	Fluorenylmethoxycarbonyl
HATU	1-[Bis(dimethylamino)methylene]-1H-1,2,3-triazolo[4,5-b]pyridinium 3-oxid hexafluorophosphate
HBTU	(2-(1H-Benzotriazole-1-yl)-1, 1, 3, 3-tetra-methyluronium hexafluoro phosphate
Ile	L-Isoleucine
IPTG	Isopropyl β-D-1-thiogalactopyranoside
Leu	L-Leucine

LMW	Low molecular weight
Lys	L-Lysine
MCM	Mobile Crystalline Materials
MSN	Mesoporous silica nanoparticles
HMSN	Hollow mesoporous silica nanoparticles
Ni-NTA	Nickel-Nitrilotriacetic acid
Pbf	2, 2, 4, 6, 7-Pentamethyldihydrobenzofuran-5-sulfonyl
PNIPAM	poly (N-isopropylacylamide)
rpm	Rounds per minute
rt	Room temperature
tBu	Tert-butyl
Trt	Triphenylmethyl, Trityl
Tyr	L-Tyrosine
SDS-PAGE	Sodium dodecyl sulfate polyacrylamide gel electrophoresis
SEM	Scanning electron microscopy
Ser	L-Serine
SPA	disulfide phenylazide
SPPS	Solid phase peptide synthesis
TEM	Transmission electron microscopy
TEMED	N,N,N’,N’-Tetramethylethylenediamine
TFA	Trifluoroacetic acid
THF	Tetrahydrofuran
TIPS	Triisopropylsilane
TMOS	Tetramethoxysilane
TRX	Thioredoxin
UV/VIS	Ultraviolet/visible light

Structure of the thesis

The following thesis contains a total of four chapters starting with an introduction providing the theoretical background of the project. Next, the general methods and experimental approaches are explained in chapter two. In the third chapter, the obtained results are analyzed and discussed in light of existing literature. The last part shall give a conclusion of all which has been done and an outlook regarding the next steps which ought to be done in the future.

Chapter 1
Introduction

1.1 Drug delivery systems

While developing a new drug, it is of essential importance to determine its way of administration to the patient. Different administration techniques are available that are classified in two major categories: systemic and local (Figure 1). When a drug is administered via local route, the drug is taken up through contact to skin or mucosal membranes after it was applied locally. By contrast, via systemic route, the drug reaches the blood stream and is thus distributed in the whole body of a patient. Systemic route can additionally be divided in enteral and parenteral methods. Enteral techniques, such as oral or rectal administration, are non-invasive and the respective drug is absorbed in the gastrointestinal tract. Oral drug administration route is frequently used as it is cheap and convenient for the patient. However, the employed drug, usually in tablet or capsule form, needs to be either stable or protected to withstand unfavorable conditions, such as acidic pH in stomach, before it reaches the gastrointestinal tract. Additionally, this way of administration can be irritating to gastric mucosa causing adverse effects such as vomiting. Another obstacle is a loss in efficacy due to the first pass effect. The first pass effect describes the hepatic metabolism of a drug absorbed from the gastrointestinal tract after its delivery to the liver. A great first pass effect means that less drug can reach the blood circulation[1–3].
When using parenteral techniques, the drug is directly applied to the blood, thus avoiding the gastrointestinal tract. Injections can be applied directly to blood veins (intravascular), in the muscle (intramuscular) and under the dermis (subcutaneous) providing a very fast access to blood circulation resulting in a faster effect for the patient when compared to oral administration. However, frequent injections may be required that cannot be

performed by the patient himself making it necessary to visit a doctor or a hospital for each injection thus decreasing patient convenience[2,4].

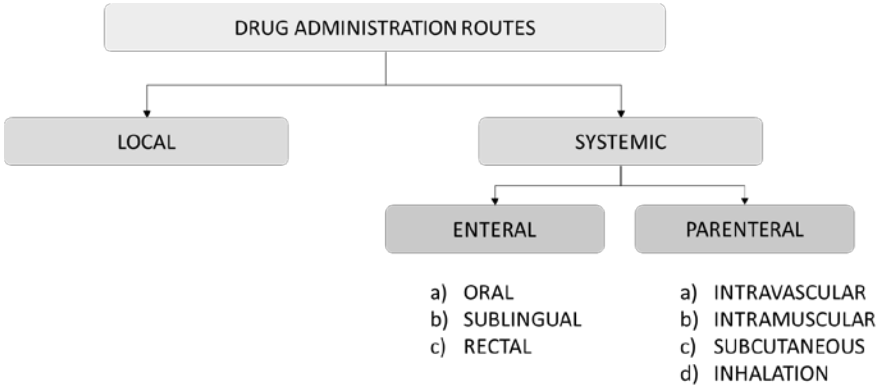

Figure 1 - Drug administration routes – Overview [1-4].

In order to protect drugs from destruction through unfavorable conditions or enzymatic degradation after administration, it is of high importance to employ effective drug delivery systems with suitable carrier materials to increase bioavailability. However, while bound to certain types of carriers, the encapsulated drug is neither active nor bioavailable[5]. Therefore, it is essential to have a proper release technique that ensures a defined drug concentration via consistent release over a certain period of time. Additional points to consider when choosing a drug delivery system are the toxicity of the carrier material and the potency of the drug. If the potency of the drug is low, a carrier system must be used which can transport large amounts of drug molecules to ensure a sufficient efficacy[5].
Two common strategies for drug delivery are the use of hydrophobic, lipid-based carrier materials e.g. liposomes (Section 1.1.1) as well as polymer-drug conjugates (Section 1.1.2). A third strategy, mesoporous silica particles, is a hot topic in current research and is investigated regarding the particle's drug carrier properties (Section 1.2).

1.1.1 Liposomes as drug carriers

Liposomes are typically built out of a phospholipid bilayer (Figure 2). The head of a phospholipid is hydrophilic and the hydrocarbon tail is hydrophobic thus resulting in a coordinated orientation of the whole membrane depending of the solvent[6]. In solution, the spherical shaped forms are favored.

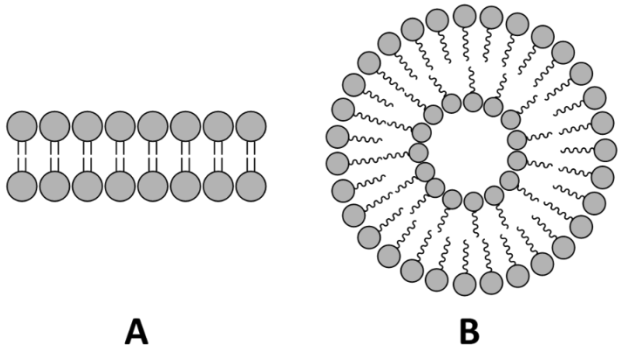

Figure 2 - Phospholipid layer types in aqueous solution;
***A**: Phospholipid membrane; **B**: Liposome.*

A typical liposome's diameter is between 50 – 1000 nm offering the possibility to be used as a drug transporting vessel through encapsulation of the active agent inside its aqueous core. Hydrophobic drugs can be transported by a liposome as well when employing special pH and gradient based loading techniques like "remote loading"[7]. While encapsulated in a liposome, the solubility of a drug, when administered to a patient, is increased[5] while the clearance of the agent is decreased at the same time[8]. This results in an increased plasma half-life of the drug. Although their capacity is size dependent, liposomes are capable to encapsulate a large amount of small drug molecules. This makes them good drug carriers for low potency drugs when a large amount of molecules are needed to reach a good efficacy[9]. Different classes of liposomes exist whereby cationic liposomes, for example, are investigated for their use in gene therapy. For this, cationic lipids with a positively charged head like DOTMA (Figure 3) are used to generate a liposome which forms a complex structure with negatively charged DNA molecules while also protecting them from degradation[10,11].

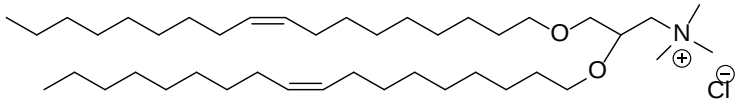

Figure 3 - Structure of the cationic lipid DOTMA.

Liposomes can further be used as an immunological adjuvant when carrying an antigen resulting in an increased immune response through macrophage activation and antibody production[12,13]. Liposomes are completely biodegradable, non-toxic and additionally reduce the toxicity of the encapsulated drug compared to the free drug[14]. Disadvantages when choosing liposomes for drug delivery are the decreased physical stability, susceptibility to dilution, low solubility of liposomes, the high production costs and a short half-life due to possible oxidation and hydrolysis reactions of phospholipids[6,15]. Although liposomes can encapsulate a high quantity of small molecules they are limited when bigger substances like proteins or peptide drugs shall be delivered. This is especially true when small liposome diameters are of interest[5]. However, the properties of a specific

liposome are dependent on the used phospholipids influencing the surface charge, the size and the preparation technique[14]. An example for a liposome-based carrier system is the encapsulation of amphotericin B for treatment of leishmaniasis[16].

1.1.2 Polymer based drug delivery

A widely known approach using polymers for drug delivery is the PEGylation of the free drug using the non-toxic polymer poly-ethylene glycol (PEG) (Figure 4)[8]. During this procedure, at least one PEG residue is attached via a linker to the drug improving its solubility in aqueous conditions. The attachment of larger PEG polymers decreases the renal clearance rate of the drug agent resulting in an increased plasma half-life, which can have a positive effect on drug efficacy[17]. In general, multiple PEG residues are attached to a molecule, peptide or protein in the course of the PEGylation reaction thus increasing molecular weight and steric shielding of the drug agent. The latter can prevent or at least decrease immune recognition of the drug compared to the free agent[8,18]. The increase of molecule size (≥ 40,000 Da) enables passive targeting abilities of e.g. PEGylated liposomes by exploit of the enhanced permeation retention effect (EPR effect)[19]. The EPR effect describes the accumulation of larger molecules and particles in hyperpermeable tumor tissues and their decreased lymphatic drainage. This effect is mainly due to the rapid tumor growth rate and can be observed as a result of the poorly developed blood vessels in tumor tissue during angiogenesis[20,21]. However, increased steric hindrance is also a big disadvantage as it can have a negative influence on drug-receptor binding: PEGylation can thus interfere with binding sites and protein structures of a protein drug agent making it less active and less effective[22]. Among other, some examples for PEGylated drugs are Pegvaliase (Phenylketonuria)[23], Pegaspargase (Acute lymphoblastic leukemia)[24] and Doxorubicin HCl liposomes (Cancer)[25]. PEGylation can be combined with liposomal delivery as asialo-erythropoietin - modified PEGylated liposomes were investigated by Ishii *et al.* for treatment of cerebral ischemia–reperfusion (I/R) injury[26].

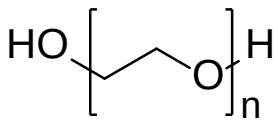

Figure 4 – Structure of the poly-ethylene glycol (PEG) monomer.

Another polymer-based drug delivery approach includes polymer microspheres which are based on natural polymers with low toxicity like cellulose or chitin (Figure 5). Although, the structure of natural, biosynthesized polymers cannot be modified equally to synthetic

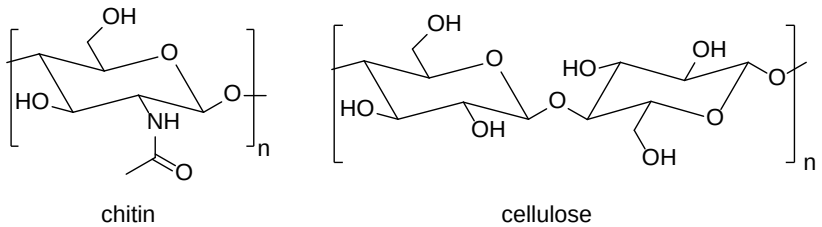

Figure 5 – Substrates for polymer-based microspheres; chitin (left) and cellulose (right).

polymers[27], natural polymers are biodegradable, that is a very important feature because the polymer carrier would have to be removed from the tissue using surgical techniques otherwise[28,29]. The microsphere's properties are dependent on the employed polymer, its weight, the sphere size and morphology as well as the synthesis procedure. The strategy for this drug carrier system is encapsulation of a free drug within the porous polymer microsphere followed by a release through passive diffusion (leaching) or through degradation of the polymer[30]. Drug substances that can be encapsulated using chitin-based nanoparticles are insulin, heparin as anticoagulant and doxorubicin for cancer therapy[31].

1.2 Silica particles

1.2.1 Synthesis of silica particles

A method for generating monodispersed silica particles was published by Stöber *et al.*[32] in 1968. The two step reaction is based on hydrolysis followed by condensation of silicic acid tetraesters such as TMOS (Figure 6)[32]. This reaction, also known as sol-gel process, was catalyzed by ammonia in a solvent mixture of alcohols and water. After the hydrolysis of TMOS to silicic acid, two silicic acid molecules condensate to a dimer by release of a water molecule. This dimer still has six hydroxy residues left that can undergo six additional condensation reactions – finally forming a silica polymer. As the polymerization reaction progresses, a dispersion of colloidal silica particles (Diameter: 1-100 nm) is generated which is widely known as sol. However, the outcome of this reaction is pH dependent. When the reaction is performed below pH 7, a gel network is generated as a result of particle aggregation whereas above pH 7 further growth of the particles is favored. The resulting particles are spherically shaped and equally sized[32–34]. The Stöber method was firstly modified by Grün *et al.*[35] by addition of a cationic surfactant which allowed the synthesis of MCM-41 type silica particles. The term MCM-41 originates from "Mobile Crystalline Materials" and describes a hexagonal mesoporous silica material characterized by pores having a diameter of 2.6 – 6 nm. The pores have a hexagonal shape facilitating entrapment of molecules[36,37]. Many other types of mesoporous silica with different pore sizes or structures have been synthesized ever since through changes in reaction conditions including the silica source used, anionic or cationic surfactants as well as structure-directing agents. Examples for mesoporous silica are also MCM-48 (cubic)[38] and MCM-50 (lamella like)[39].

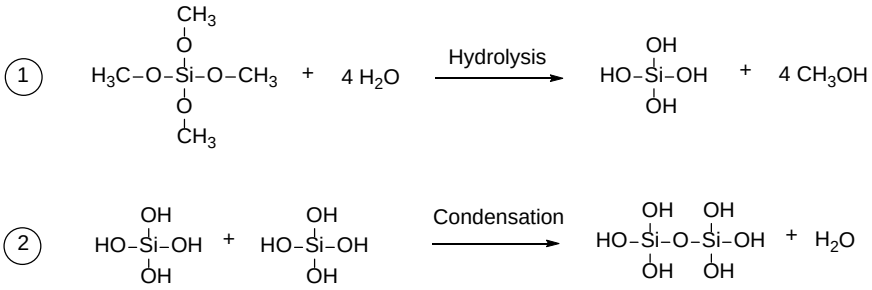

Figure 6 - Schematic reaction pathway of silica particle synthesis using the sol-gel process: ***1)*** *Hydrolysis of TMOS;* ***2)*** *Condensation of silicic acid, adapted from [32].*

1.2.2 Mesoporous silica nanoparticles as drug carrier

Mesoporous silica nanoparticles (MSN) are synthesized using e.g. the sol-gel process as previously described in 1.2.1. The covalent bond between silicon and oxygen is strong resulting in a high resistance versus (bio)degradation[40]. MSNs have a hydrophobic core and an active hydrophilic surface that is completely covered by silanol groups. They are particularly characterized by their porous structure providing a large pore volume and hence a higher drug loading capacity when compared to liposomes. Additionally, the silanol groups present on their internal and external surface allow for a wide variety of different functionalizations (Figure 7)[36], which can influence the drug loading and releasing properties of MSNs[40]. Besides that, the synthesis of a different kind of MSNs such as hollow mesoporous silica nanoparticles (HMSN) can also improve drug loading capacities by 3 to 15 times[36]. This special form is characterized by a larger hollow cavity inside the particle providing more space for drug entrapment[41]. She *et al.*[42] improved this uptake further using electrostatic attractions by functionalization of the silanol groups of HMSNs with silanes such as (3-aminopropyl) triethoxysilane (APTES). The loading of a negatively charged molecule was increased because of the thus generated positive charges on the HMSN's surface[42]. As the drug loading capacity depends on pore volume, it is also possible to expend this volume using pore swelling agents such as triisopropyl benzene (TIPB)[43]. However, the encapsulated drug is not active and has to be released from the MSN mainly depending on passive diffusion of the molecule out of the pore. Molecules that have less interaction with the surface are not retained and can therefore be easier released and vice versa. Wang *et al.*[44] describe a controlled release behavior with modifications of the silanol groups using APTES. When MSNs were first loaded with a molecule and functionalized with APTES afterwards, it was observed that the molecules in the pores remained in the particle. If the particle was first functionalized and then loaded, the molecule was mainly adsorbed to the pore-free surface and a very fast release was reported[44]. Cheng *et al*.[45] were able to generate tri-functionalized mesoporous silica nanoparticles with combined imaging, targeting and therapy properties. To achieve this, they incorporated a fluorescent contrast agent in the silica structure for imaging, whereas for specific targeting, they functionalized the particle surface with peptides binding to certain integrins which are overexpressed in cancer cells.

The therapeutic effect was achieved with a palladium-porphyrin based photosensitizer entrapped in the pores. Cheng *et al.* were able to confirm a specific targeting and an excellent therapeutic effect[45]. Current research fields for mesoporous silica nanoparticles in biomedicine, in particular cancer therapy, are HMSNs with doxorubicin[46] and MCM-41 with quercetin[47].

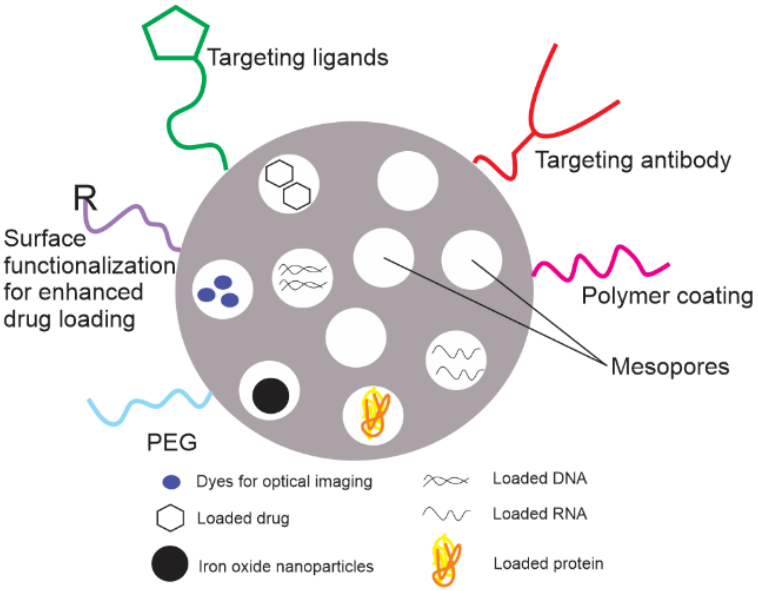

Figure 7 - Mesoporous silica nanoparticle, functionalizations overview (surface functionalizations can also be found in the particle pores), adapted from [36].

1.3 Biomimetic silica

1.3.1 Diatoms - silica precipitating organisms

Silica structures cannot only be produced by chemical synthesis but are also an essential part of living organisms. *Bacillariophyta*, also known as diatoms, are unicellular, photosynthetic eukaryotes with a typical length between 2-200 µm. Diatoms can be found in the oceans as well as in fresh water. More than 10,000 known species representatives are characterized by the shape and structure of their silicon-based cell wall[48]. The cell wall (Frustule) is built out of hydrated amorphous silica ($[Si_nO_{2n-(nx/2)}(OH)_{nx}]$, $x \leq 4$)[49] generated by the diatom. For this, silicic acid, which originates from weathered silicate, is taken up via silicic acid transporter proteins[50] and transported through the cytoplasm to silica deposition vesicles (SDV)[51,52]. The polymerization reaction is highly controlled to avoid a premature formation of silica inside the cell[48,53]. The thus formed cell wall (Frustule) can be divided in two halves: the upper half known as epitheca and the lower half called hypotheca. Both halves contain a capping valve and multiple girdle bands. The epitheca is bigger when compared to the hypotheca and overlaps with it forming a petri dish like shape (Figure 8, top) while enclosing the protoplast[54]. In reference to the shape and symmetry of the frustule, two types of diatoms can be distinguished: circular shaped centric diatoms with radial symmetry and protracted pennate diatoms with bilateral symmetry[55].In order to reproduce, the protoplast divides into two daughter cells via mitosis followed by cytokinesis. Both daughter cells are still present in the original frustule of the mother cell. A new epi- and hypotheca has to be build, so both cells can separate from each other (Figure 8, bottom). This is done by the previously mentioned SDVs which precipitate silica while expanding. Once silica precipitation is finished and new girdle bands were formed, both cells can divide completely forming two new diatoms[51,52].

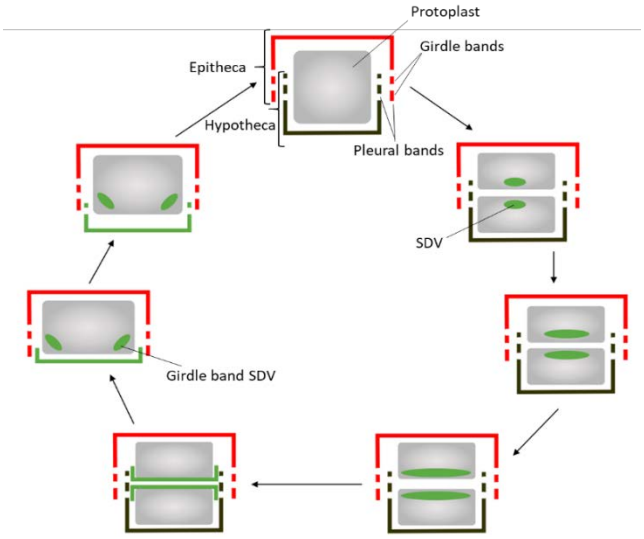

Figure 8 – Morphology and life cycle of diatoms, adapted from [51-54].

1.3.2 Silaffins

The formation mechanism of the diatom's silica-based cell wall drew much attention. Proteins showing a high affinity to silica were extracted from *Cylindrotheca fusiformis* and named silaffins[56]. This term includes the proteins silaffin-1 A (4 kDa), silaffin-1 B (8 kDa) as well as silaffin-2 (17 kDa). Based on a cDNA library of *C. fusiformis*, the responsible gene *sil1* was cloned followed by the identification of the amino acid sequence of the respective precursor protein sil1p (Figure 9)[56]. Sil1p contains a signal sequence on its N-terminal part between amino acids 1 and 19 followed by amino acids 20 to 107. The first part's function is translocation into the endoplasmatic reticulum (ER) whereas the role of the latter is still not known. The C-terminal part is highly repetitive, contains a large number of lysine residues and can be divided in seven units named R1 to R7. Silaffin proteins are derived from that precursor protein and can be allocated to certain units e.g. silaffin-1 B which results from R1 and silaffin-1 A_1 (Figure 9A) which originates from units R3 to R7[52,56,57]. Silaffin-1 A_1 exhibits a large number of posttranslational modifications which influences the overall charge of the peptide. In particular, the amino acid lysine gets modified either with N-methylated oligopropylenimine (Figure 10A, violet) or through di- or trimethylation (Figure 10A, red). After oxidation of the lysine residue, is also can be modified by phosphorylation at δ-position. Additionally, all serine amino acids are phosphorylated (Figure 10A, green)[52,56,57]. All silaffins generate silica directly proportional to their quantity used through coprecipitation in silicic acid. It was found that serine phosphorylations play a key role in the process because no precipitation was observed in their absence. Nevertheless, as long as phosphate ions are present in the precipitating solution, e.g. through buffer, the lack of serine phosphorylation did no longer limit the precipitation properties[52,57,58]. The absence of negatively charged phosphate modifications or ions changes the self-assembly properties of the peptides[58]. This process is important for the silica precipitating activity because it facilitates a high local amino group concentration to catalyze siloxane bond formation[59]. A silicic acid molecule donates a proton to a deprotonated amino group thus generating a negatively charged oxygen which further attacks a second silicic acid molecule via a nucleophilic attack. The second silicic acid molecule loses a water molecule during the condensation reaction which is facilitated by another protonated amino group. As the reaction progresses, silica is formed (Figure 10B)[60].

```
        MKLTAIFPLLFT                12
        AVGYCAAQSIADLAAANLS         31
        TEDSKSAQLISADSSDDAS         50
        DSSVESVDAASSDVSGSSV         69
        ESVDVSGSSLESVDVSGSS         88
        LESVDDSSEDSEEEELRIL        107
R1      SSKKSGSYYSYGTKK            122
           SGSYSGYSTKKSASRRIL      140
R2      SSKKSGSYSGYSTKKSGSRRIL     162
R3      SSKKSGSYSGSKGSKRRIL        181
R4      SSKKSGSYSGSKGSKRRNL        200
R5      SSKKSGSYSGSKGSKRRIL        219
R6      SSKKSGSYSGSKGSKRRNL        238
R7      SSKKSGSYSGSKGSKRRIL        257
        SGGLRGSM                   265
```

Figure 9 – Amino acid sequence of silica precursor protein si11p (265 amino acids); Signal Peptide 1-19 (italics), Repetitive parts R1 to R7 (bold), Lysine highlighted in grey, adapted from [56]

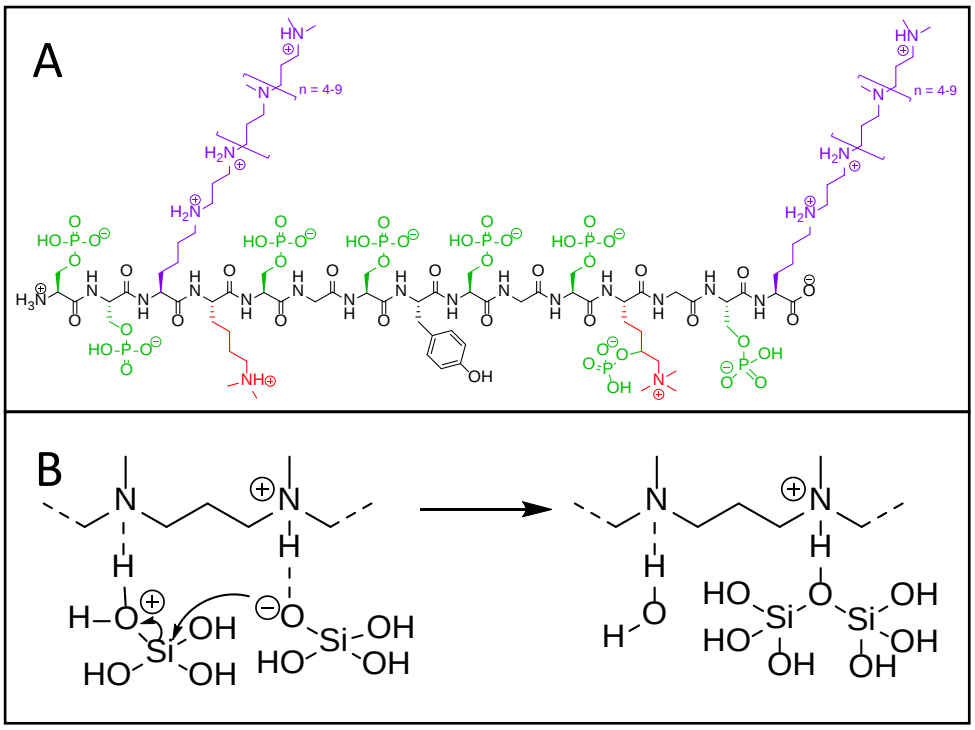

*Figure 10 – **A**: Structure of native silaffin-1 A_1 at pH 5; derived from Cylindrotheca fusiformis; green: phosphate modification, violet: N-methylated oligopropylenimine residue, red: methylated lysine residues, adapted from [55-57]; **B**: Proposed mechanism of silaffin mediated polycondensation of silicic acid in the course of silica precipitation, adapted from [60].*

1.3.3. Silica precipitation with the R5 peptide

Biomimetic silica particle formation employing peptide R5 (Figure 9, (H-SSKKSGSYSGSKGSKRRIL-OH) is most probably mediated by the lysine residues of the peptide because R5 lacks post-translational modifications present in native silaffins[61]. Lechner *et al.*[62] synthesized 6 different variants of R5 containing varying modifications such as trimethylated lysine, ε-(4-spermidine) succinyllysine, phosphoserine and 7-nitro-2,1,3-benzoxadiazole. All experiments described by Lechner *et al.* were carried out at pH 7 using phosphate buffer. The results show, that the unmodified peptide R5 as well as the trimethyl lysine variant exhibited a good silica precipitation activity resulting in homogenous, spherical silica particles with an average diameter of 750 nm. Other modifications, such as single and global serine phosphorylation, interfered with the dimerization of the R5 peptide and thus silica precipitation activity due to electrostatic repulsion. They were able to show that side chain modifications are able to influence the precipitation activity of R5 as well as morphology of the resulting silica particles[62].

Buckle *et al.*[63] also investigated side chain modification and their influence on precipitation activity as well as silica particle size. For this, they synthesized three different modified R5 variants with trimethylation either at lysine K3, lysine K4 or both lysine

residues. They found that the maximum activity for silica precipitation (nmol SiO2 / µmol peptide in 5 min) decreased for all three variants when compared to unmodified R5 while this decrease was strongest for the peptide methylated at K3 and K4. However, silica precipitation using each variant resulted in silica particles with a larger mean diameter (714 ± 95 nm, K3 trimethylated) compared to unmodified R5 (594 ± 93 nm)[63].

In further experiments, Lechner *et al*.[64] attached two proteins, eGFP (enhanced green fluorescent protein) and TRX (thioredoxin) to four different R5 variants via expressed protein ligation (EPL). They were able to obtain spherical shaped silica particles after precipitation when using the unmodified eGFP-R5 variant. These particles were bigger with a diameter of approximately 1 µm when compared to the unmodified R5 precipitated silica particles with approximately 750 nm diameter[64]. Images taken of this silica particles with fluorescent microscopy proved the presence of eGFP. For the unmodified TRX-R5 conjugate, Lechner *et al*.[64] obtained silica particles which appeared to be even bigger than 1 µm in diameter. Activity of the TRX enzyme was determined using insulin and a spectrophotometer at a wavelength of 650 nm. They could see that the activity of immobilized TRX-R5 was higher in comparison to the free peptide TRX conjugate[64].

It is also possible to immobilize enzymes that are not attached to R5 during silica precipitation. Edwards *et al.*[65] were able to successfully immobilize human carboxylesterase 1 (*h*CE1) in biomimetic silica. For their incubation experiments, a mixure of 1 M TMOS solution, 100 mg/mL R5 solution and a 0.1 M potassium phosphate buffer pH 7.4 containing *h*CE1 was incubated at 22°C for 10 min. Encapsulation of the enzyme was determined by activity measurements of the supernatant and the silica particle suspension after incubation. The supernatant showed no activity while the silica particle suspension displayed a decreased activity compared to the *h*CE1 in solution. Edwards et al. were able to demonstrate that *h*CE1 was successfully incorporated into R5 silica particles[65].

In 2017, Bräuer *et al*.[66] investigated the accessibility of both C- and N-terminal parts of the peptide R5 inside silica particles. For this, two R5-biotin conjugates were synthesized bearing biotin either at the C-terminal or N-terminal part of the amino acid chain. Bräuer *et al*. were able to precipitate silica particles using both variants of R5-biotin[66]. The generated silica particles were incubated with a streptavidin-gold nanoparticle conjugate or an avidin-sulforhodamine 101 conjugate that should bind to biotin-R5, if accessable, at both termini. The results obtained by Bräuer *et al*. showed that both conjugates attached to both types of silica particles. However, the streptavidin and avidin conjugates were also adsorbed to silica particles, precipitated with unmodified R5. Due to the fact that an unspecific adsorption of both conjugates to R5 silica particles in absence of biotin was observed, they concluded that it was not possible to determine whether the C- and N-termini of R5 were accessible inside the silica particle or not[66].

1.4 Green fluorescent protein (GFP)

The first used protein for the adsorption studies performed in this work is the green fluorescent protein (GFP) that was firstly described by Shimomura *et al*. in 1962[67]. GFP is built out of 238 amino acids (Figure 11, left) with a total molecular weight of 26,900 Da[68]. It was firstly cloned and expressed using the genes of the jelly fish *Aequorea victoria*[69,70]. A 3D model of a GFP variant shows, that GFP is basically a barrel built of eleven β-strands arranged in a β-sheet (Figure 11, right). An α-helix in the center consists of a hexapeptide, which forms the chromophore 4-(p-hydroxy benzylidene)-imidazolidin-5-one[71]. This chromophore was discovered by Shimomura *et al.* in 1979[72]. It is formed out of six amino acids of the GFP chain in an intramolecular, autocatalytic cyclisation reaction. This is very unique because this reaction does not require a cofactor or additional substrates[73]. The respective amino acids are Phe64-Ser-Tyr-Gly-Val-Gln69 but only three amino acid residues are responsible for the emission of green light. These residues are Ser65 - dehydroTyr – Gly67. Two excitation peaks are described for GFP at 395 nm (major) and 475 nm (minor) while fluorescence emission can be measured at 509 nm in the form of a green light[74]. Nowadays, GFP is a common and frequently used protein in cell biology for imaging of biochemical processes such as signal transduction[75] and gene expression[76].

```
        10         20         30         40         50
MSKGEELFTG VVPILVELDG DVNGHKFSVS GEGEGDATYG KLTLKFICTT
        60         70         80         90        100
GKLPVPWPTL VTTFSYGVQC FSRYPDHMKQ HDFFKSAMPE GYVQERTIFF
       110        120        130        140        150
KDDGNYKTRA EVKFEGDTLV NRIELKGIDF KEDGNILGHK LEYNYNSHNV
       160        170        180        190        200
YIMADKQKNG IKVNFKIRHN IEDGSVQLAD HYQQNTPIGD GPVLLPDNHY
       210        220        230
LSTQSALSKD PNEKRDHMVL LEFVTAAGIT HGMDELYK
```

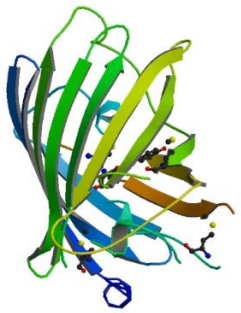

*Figure 11 – **Left**: Amino acid sequence of GFP, Source: UniProtKB - P42212 (GFP_AEQVI); **Right**: Structure of a variant of GFP, 1EMA, from organism Aequorea victoria, Source: https://www.rcsb.org/structure/1EMA, 23.09.2019.*

1.5 Thioredoxin (TRX)

The second used protein for adsorption studies is thioredoxin as it should be investigated whether an enzyme is still active while adsorbed onto silica particles. The term “thioredoxin” does not refer to a single protein but is used for a whole 12,000 Da redox protein class which can be found in nearly all kind of organisms. In 1964, the first thioredoxin was purified from *E. coli* by Laurent *et al*.[77]. One example of this protein class is thioredoxin-S_2 from *E. coli* which is built out of 108 amino acids (Figure 12). Its active center (-Trp-Cys-Gly-Pro-Cys-Lys-) lies in between a five stranded β-sheet with four adjoined α-helices[78]. Both Cysteine in this sequence are vital for its function as a redox

protein involved in e.g. regulation and signaling processes[79]. The enzyme thioredoxin reductase catalyzes the reduction of the disulfide in thioredoxin-S_2 in presence of NADPH. The reduced form of thioredoxin-$(SH)_2$ serves in the following reaction as a hydrogen donor for ribonucleotide reductase during deoxyribonucleotide formation for DNA synthesis[77,78]. However, the thioredoxin system is a disulfide reductase not only during this particular reaction but in general: Insulin for example consists of two chains connected by two interchain disulfides. When thioredoxin destroys this connection after reduction of the disulfide bonds the B chain aggregates and precipitates resulting in a turbid solution. This turbidity can be measured at 650 nm using a spectrophotometer[80] serving as an assay to determine TRX activity.

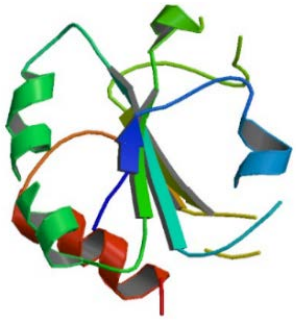

Figure 12 - Structure of thioredoxin-S_2 from Escherichia coli, 1SRX, P0AA25Source: http://www.rcsb.org/structure/1SRX, 11.11.2019.

1.6 Aim of the thesis

In this project, biomimetic silica particles shall be investigated with a focus on their possible protein carrier properties. Silica particle synthesis will be done using peptides R5 and a Cy5-R5 conjugate. The morphology of both silica particle types will be analyzed with scanning electron microscopy (SEM). Evaluation of their protein adsorption properties will be carried out while employing the enhanced green fluorescent protein (eGFP) and thioredoxin (TRX), followed by a release of the adsorbed cargo. Adsorption of eGFP and TRX onto silica particles will be investigated by incubation in protein solutions using 50 mM potassium phosphate buffer with different protein concentrations. Release of the adsorbed proteins will be monitored using the same buffer at different pH values. The supernatants obtained after adsorption and release experiments will be analyzed using an HPLC system. The adsorbed and released amount of protein will be determined based on the peak area at 214 nm. Additionally, emission measurements at the respective wavelength of Cy5 or eGFP will be conducted using a plate reader.

Chapter 2
Materials and Methods

2.1 General protocols

2.1.1 Peptide and protein identification / quantification using HPLC

The peak areas for identification as well as quantification of peptides and proteins were determined using a Dionex UltiMate System 3000 with UV detector. Absorption and the respective peak areas were determined at 214 nm and 280 nm for compound **4**, compound **6**, the enhanced green fluorescent protein (eGFP) and thioredoxin (TRX).

2.1.2 Fluorescence measurement

Fluorescence detection for identification of eGFP and compound **6** was carried out using a Biotek Synergy Mx plate reader adjusted at the excitation and emission wavelength of each substance (Table 1). Compound **6** was measured using the same settings as recommended for the pure fluorescence dye cyanine-5. A 96 well plate was used with 100 µL solution in each well. Prior to each measurement, a blank was measured which was then subtracted from each obtained sample value.

*Table 1 – Excitation and emission wavelength for fluorescence measurement of eGFP and compound **6** with plate reader.*

Substance	Excitation wavelength (nm)	Emission wavelength (nm)
EGFP	395	509
Compound 6	620	670

2.1.3 Preparation of SDS-PAGE gels

For SDS-PAGE (Sodium dodecyl sulfate polyacrylamide gel electrophoresis) all gels were prepared using the standard protocol (Table 2). First, the separating gel was prepared and then transferred into a multi-casting chamber for polymerization. After 30 min, the stacking gel was cast on top of the separating gel and the loading bags for each gel were formed using a comb with 10 teeth. The thus polymerized gel was loaded with samples previously treated with the 2x sample buffer (Table 3) and heated at 95 °C for 5 min. For protein identification a low molecular weight (LMW) protein standard marker purchased in the LMW calibration kit for SDS electrophoresis from Amersham (Lot: 16953347,

Table 4) was used. Electrophoresis was carried out with an Elektrophorese Mini Protein Tetra Cell by BioRad. After that, all gels were stained using a coomassie staining solution and destained using methanol/water with acetic acid (Table 5). For gel imaging a BioRad ChemiDoc MP Imaging System was utilized.

Table 2 – Preparation protocol of separating and stacking gel for SDS-PAGE, fits for 9-12 gels.

Substance (volume)	Separating gel	Stacking gel
ddH_2O (mL)	12.5	12.5
1.5 M TrisHCl, 0.4% (w/v) SDS, pH 8.8 (mL)	13.5	-
0.5 M TrisHCl, 0.4% (w/v) SDS, pH 6.8 (mL)	-	2.5
30% Acrylamide (mL)	26.0	3.5
10% SDS (µL)	550.0	185.0
10% APS (µL)	550.0	185.0
TEMED (µL)	18.0	18.0

Table 3 - Protocol for 2x sample buffer preparation.

2x sample buffer, 500 mM Tris, pH 6.8	% (w/v)	% (v/v)
SDS	6.00	-
Glycerin	-	35.00
Bromophenolblue	0.05	-
β-Mercaptoethanol	-	3.55

Table 4 – Ingredients of the protein standard marker, LMW, Amersham.

Protein standard marker, LMW	M (kDa)	R_f
Phosphorylase b	97.0	0.07
Albumin	66.0	0.13
Ovalbumin	45.0	0.25
Carbonic anhydrase	30.0	0.46
Trypsin inhibitor	20.1	0.67
α-Lactalbumin	14.4	0.89

Table 5 – Preparation of coomassie staining and destaining solution.

Coomassie staining solution	V (mL)	m (g)
Coomassie R250	-	1
Acetic acid	100	-
Methanol	450	-
ddH_2O	450	-
Destaining solution	**V (mL)**	**m (g)**
Acetic Acid	100	-
Methanol	400	-
ddH_2O	500	-

2.1.4 Sample preparation for scanning electron microscopy

For scanning electron microscopy (SEM), 2 µL of a silica suspension in water was applied to a ThermanoxTM coverslip and subsequently dried overnight. The resulting sample was then coated with gold while in high vacuum using a Bal-Tec SCD 005 coater. For imaging a Zeiss SEM Supra 55 VP operating at 20 kV was employed.

2.1.5 Activity measurement of thioredoxin (TRX)

The enzymatic activity of thioredoxin after expression was verified using a Nanodrop 2000c spectrophotometer in cuvette mode. For this, three solutions were prepared: First, a 1 mM insulin solution with 2 mM EDTA in a 100 mM phosphate buffer at pH 6.5[64]. To dissolve the insulin completely, a few drops of 1M HCl were added. Second, an always freshly prepared 20 mM DTT stock solution and last, a 2 mM EDTA solution both in phosphate buffer. In order to measure the activity of TRX, 5 µL of the insulin solution, 5 µL of the DTT solution, 17 µL of a 0.7 mg/mL TRX solution and 73 µL of the 2 mM EDTA in phosphate buffer were mixed in a cuvette to a total volume of 100 µL. The TRX solution was prepared by dilution of the obtained product after expression and purification (Section 2.5) to give a final concentration of 10 µM TRX in the cuvette. The absorbance was then measured at 650 nm for 20 min. As blank, a mixture without DTT was used.

2.2 Solid phase peptide synthesis of Cys-R5 (R5)

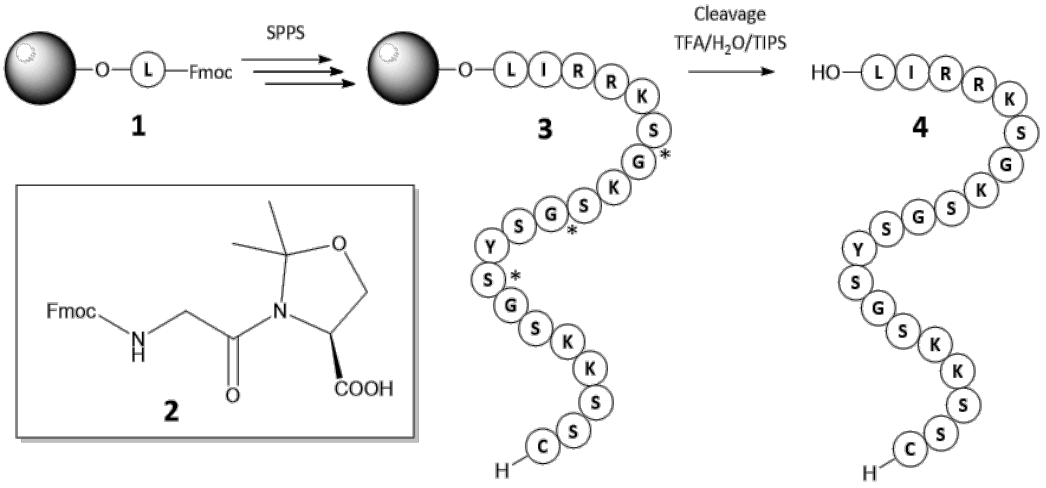

*Figure 13 – Schematic reaction pathway for solid phase peptide synthesis of Cys-R5 (**4**) via the Fmoc method; **2**: Structure of the pseudoprolin amino acid building block Fmoc-Gly-Ser(psiMe,Mepro)-OH, used three times (*).*

Solid phase peptide synthesis (SPPS, Figure 13) of the 20-mer Cys-R5 (**4**) with a calculated mass of 2116.42 Da was performed manually using Fmoc-Leu-Wang-resin (**1**, 100-200 mesh, 0.69 mmol/g, Novabiochem®) at a scale of 0.1 mmol. First, the resin was prepared by washing with both DCM and DMF in a 10 mL syringe for 5 min, followed by incubation in DMF in order to allow swelling of the resin for 30 min. After that, the Fmoc protecting group was removed using a solution of 20% piperidine in DMF for 3 min and 7 min reaction time. The resin was then washed three times with 10 mL DMF before the first activated amino acid (aa) was added. For this, 5 eq aa (Table 6) were dissolved in freshly prepared HBTU/DMF solution (4.8 eq HBTU in 1 mL DMF). For aa activation, 10 eq (180 µL) DIPEA were added to the mixture which was subsequently transferred to the resin. After 30 min of coupling, the resin was washed three times with DMF followed by the Fmoc deprotection of the recently coupled amino acid. The cycle was repeated until the last amino acid was attached to the growing peptide chain. The resin was washed five times with 10 mL DMF, one time with DCM and MeOH each and dried under reduced pressure to obtain compound **3**. The peptide was cleaved off the resin by using 10 mL/g(resin) of a cleavage solution containing 95% TFA, 2.5% ddH_2O and 2.5 %TIPS for 4 h. Subsequently, the solution container was filled up with at least the triple volume of ice-cold diethylether for product precipitation. This was centrifuged at 4,000 rpm and 4 °C for 5 min using a refrigerated centrifuge Sigma 3-16 PK. Afterwards, the supernatant was removed and the peptide pellet was washed with ice-cold diethylether twice and air dried in the hood. Last, the peptide was dissolved in a 1:1 mixture of ACN and ddH_2O with 0.1% TFA for immediate lyophilization in order to obtain the crude peptide **4**.

*Table 6 – Approach for manual synthesis of compound **4**; List of all employed L-amino acid building blocks, their respective abbreviations, molecular weight and used amounts for overall synthesis.*

Amino acid building block	Abbreviation	Molecular weight (g/mol)	Calculated amount (mg)
Fmoc-Ile-OH	I	353.4	176.7
Fmoc-Arg(Pbf)-OH	R	648.8	648.8
Fmoc-Lys(Boc)-OH	K	468.5	937.2
Fmoc-Gly-Ser(psiMe,Mepro)-OH	GS	424.5	636.6
Fmoc-Tyr(tBu)-OH	Y	459.5	229.8
Fmoc-Ser(tBu)-OH	S	383.4	766.8
Fmoc-Cys(Trt)-OH	C	585.7	292.9

2.2.1 Purification of the crude Cys-R5 (R5)

The crude peptide **4** was purified with a Waters Prep 150 HPLC system using a Kromasil 300-10C18 column (Dim: 21.2x250 mm) with a gradient of 5-55% eluent B in 50 min at 20 mL/min flowrate. When a semi-preparation column was employed a Kromasil 300-10C18 column with 10x250 mm dimensions and a gradient of 5-45% eluent B in 30 min with 10 mL/min flowrate was used. Utilizing a Waters 2767 Sample Manager with a Waters 3100 Mass Detector the calculated mass/charge values of m/z = 1059.21, m/z = 706.48 and m/z = 530.11 were collected in fractions and further analyzed via direct injections. This was then pooled and lyophilized overnight.
Compound **4** was successfully synthesized and purified with a total yield of 27% referred to the used amount of resin. Final analysis was done employing a Dionex UltiMate 3000 HPLC system with 5-65% eluent B in 30 min with 1 mL/min flowrate using a C18 column (Section 3.1). A list of the employed eluents can be seen in Table 7.

*Table 7 - Eluent preparation for purification and final analysis of compound **4** using Waters and Dionex HPLC systems.*

Eluent contents	Waters	Dionex
Eluent A	ddH_2O + 0.05% TFA	ddH_2O + 0.1% TFA
Eluent B	ACN + 0.05% TFA	ACN + 0.1% TFA

2.3 Solid phase peptide synthesis of Cy5-R5

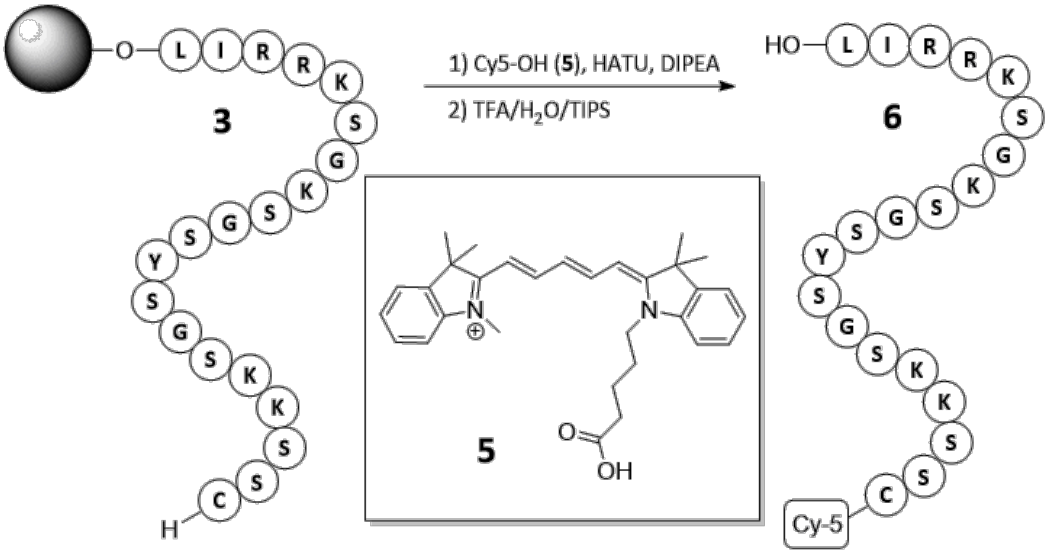

*Figure 14 – Schematic reaction pathway for the conjugation of the fluorescence dye Cy5 (**5**) with the resin attached R5 (**3**).*

The synthesis of **6** with a calculated mass of 2566.4 Da (Cy5-R5, **6**, Figure 14) was carried out in a 0.01 mmol scale using dry resin **3**, which was previously swollen in DMF for 30 min. For conjugation, 4 eq of the dye cyanine-5 were dissolved in 3.5 eq (70 µL) of a 0.5 M HATU/DMF solution which was freshly prepared. To this, 10 eq (17 µL) DIPEA were added and the mixture was filled up with DMF to a total volume of 1 mL. The syringe with the reaction mixture was placed onto a rotator overnight. The reaction mixture was removed and the resin was washed three times with DMF, one time with both DCM and MeOH and air dried for 30 min. Peptide cleavage was performed onto the rotator using 95% TFA with 2.5% TIPS and 2.5% ddH_2O for 4 h. The supernatant was removed and ice-cold diethylether was added to precipitate the crude peptide conjugate. This was centrifuged using a refrigerated centrifuge (Sigma 3-16 PK, 4°C, 4,000 rpm, 5 min) and washed two additional times with ice-cold diethylether. The resulting peptide pellet was dried with argon and dissolved in a mixture of 1:1 ACN and ddH_2O with 0.1% TFA for lyophilization.

2.3.1 Purification of the crude Cy5-R5

Peptide **6** was purified using the same equipment and settings which were employed for purification of **4** in a semi-preparative approach. The mass/charge values of m/z = 642.6 and m/z = 856.5 were collected yielding blue colored fractions which were analyzed via direct injections afterwards, pooled and lyophilized overnight. Compound **6** was successfully synthesized manually with an isolated yield of 15% referred to the used

amount of resin. The final analysis (Section 3.2) was done similar as described for **4** in 2.2.1.

2.4 Biomimetic silica particle formation

2.4.1 Formation of silica particles using compound 4

Silica particle precipitation was performed using a 1 mg/mL solution of **4** in 50 mM potassium phosphate buffer at pH 7 as well as a 4% TMOS solution in 1 mM HCl. The 4% TMOS solution was always freshly prepared and incubated at room temperature (rt) for 4 min before both solutions were mixed in a ratio of 1:9 (TMOS:**4**). This was further incubated in the hood for 30 min. A schematic workflow of this procedure is shown in Figure 15. Next, the obtained silica particle suspension was centrifuged with an Eppendorf centrifuge 5418 230 V/50-60 Hz at 14,000 rpm at rt for 5 min or with a Beckman Coulter Allegra X-30R centrifuge at 4,000 rpm at rt for 5 min. The supernatant was removed and the silica particles were suspended in ddH_2O and washed twice followed by centrifugation. The particles were suspended in 50 mM phosphate buffer at pH 7 to yield a 4 mg/mL suspension. This was calculated using the amount of applied **4** which usually doubles its weight during silica particle synthesis. The synthesized particles were prepared as described in 2.1.4 and further analyzed with SEM measurement (Section 3.3.1).

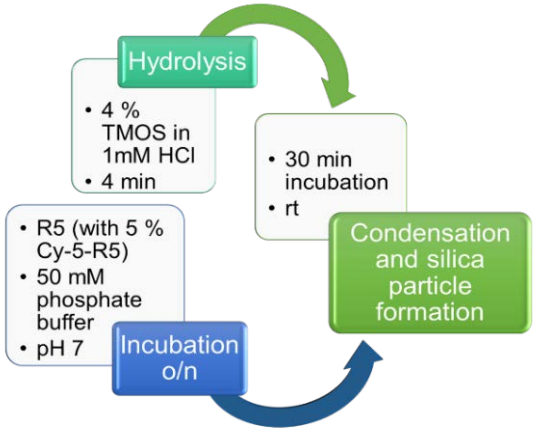

Figure 15 - Schematic workflow for silica particle formation.

2.4.2 Formation of Cy5-R5 silica particles using compound 6

Silica particle precipitation using **6** was done similar to the silica particle formation using **4** (Section 2.4.1). However, the 1 mg/mL solution of compound **4** was replaced with a 1 mg/mL mixture containing 95% of compound **4** and 5% of compound **6**. The remaining conditions were kept the same yielding blue colored silica particles. These particles were treated as discussed in 2.1.4 and subsequently analyzed via SEM imaging (Section 3.3.2).

2.5 Protein expression and purification of eGFP and TRX

2.5.1 Expression of eGFP and TRX

Bacterial growth of either *E. coli* strains BL21/pEGFP (AMP^R) for eGFP or Rosetta 2 with pTXB3-Trx-Mxe-H6-CBD for TRX expression (Table 8) was initiated in 2YT medium (Table 9) for each protein with a concentration of 100 µg/mL ampicillin. In the course of TRX expression, additionally 30 µg/mL chloramphenicol was added to the medium (Table 10). This was incubated at 37 °C while shaking overnight using an Infors HT Multitron incubator. The next day, a main culture of autoclaved 2YT medium was prepared for each protein separately with the same antibiotic concentrations as described above and subsequently mixed with the respective turbid overnight culture in a ratio of 10:1. The media were incubated at 37 °C while shaking until the optical density was between 0.6 and 0.8 AU in order to achieve an optimal cell quantity for protein expression. Therefore, a sample was taken for monitoring of the cell growth after every 30 min and measured *via* a Nanodrop 2000c spectrophotometer from Thermo Scientific (cuvette mode, cell cultures, λ= 600 nm). Once the desired optical density was reached, the IPTG stock solution was added to the media to reach a final concentration of 240 µg/mL IPTG for eGFP and TRX to start protein expression. For eGFP, the medium was incubated for 4 h while the TRX medium was incubated for 2 h, both at 37 °C while shaking. Expression was monitored via SDS-Page.

Table 8 – Bacteria strains employed for protein expression of eGFP and TRX.

Protein	Bacteria strains
eGFP	BL21/pEGFP (AMP^R)
TRX	Rosetta 2 with pTXB3-Trx-Mxe-H6-CBD

Table 9 – Protocol for 2YT-medium preparation for protein expression.

Substance	Concentration (g/L)
Tryptone	16
Yeast extract	10
NaCl	5

*Table 10 – Antibiotic and IPTG stock solution concentrations and the respective final concentration in medium; *:Chloramphenicol was not employed for eGFP expression but for TRX expression.*

Substance	Stock solution	Final concentration in medium
Ampicillin	100 mg/mL in ddH_2O (sterile filtered)	100 µg/mL
Chloramphenicol*	30 mg/mL in ethanol (sterile filtered)	30 µg/mL
IPTG	240 mg/mL in ddH_2O	240 µg/mL

Next, the *E. coli* suspensions were centrifuged at 4°C and 6,000 rpm for 30 min using a Beckman Coulter Avanti J-226 XP centrifuge. The resulting supernatants were removed and each pellet suspended in 40 mL 1x TBS (50 mM Tris, 150 mM NaCl, pH 7.6) for eGFP or 1x PBS pH 7.4 for TRX. Afterwards, the cells were disrupted twice using a Constant Systems TS cell disruption system at 10 °C and 1.9 kbar. The cell lysates were centrifuged at 4 °C and 25,000 rpm for 30 min yielding cell pellets and supernatants. Both proteins were found in their respective supernatant which was directly used for further purification. The cell pellet was disposed of in both cases.

2.5.2 Purification of eGFP and TRX

The supernatants obtained after protein expression of eGFP and TRX were loaded separately onto a 5 mL His Trap™ Ni-NTA column using a ÄKTA Prime Plus from Amersham Biosciences with a flowrate of 1 mL/min. The flowthrough was collected and a sample was taken once the UV trace reached the maximum intensity. The loaded column was then washed with eluent A (Table 11). Elution was carried out using a gradient of 0-100% eluent B over 60 min at a flowrate of 1.5 mL/min. Fractions were collected with an autosampler and analyzed via SDS-PAGE.

Table 11 – Ni-NTA eluents employed for eGFP and TRX purification, Eluent A: washing eluent, Eluent B: elution eluent.

Ni-NTÄ eluents	EGFP	TRX
Eluent A	1x TBS, 10 mM imidazole, pH 8	1x PBS, pH 7.4
Eluent B	1x TBS, 300 mM imidazole, pH 8	1x PBS, 500 mM imidazole, pH 7.4

All fractions containing purified protein were pooled and transferred to a dialysis tube Spectra/Por with a 6,000 - 8,000 Da cutoff. For eGFP, dialysis was carried out using 50 mM potassium phosphate buffer at pH 7 overnight. A second dialysis was performed afterwards with fresh buffer for 6 h. After that, the eGFP solution was centrifuged at 4 °C and 3,500 rpm for 10 min using a Beckman Coulter Allegra X-30R centrifuge. The resulting eGFP supernatant was diluted to a concentration of 1 mg/mL and stored at -80 °C.

For TRX, 1x PBS at pH 7.4 was used for overnight dialysis. After that, the purified TRX full-length construct was cleaved using a 1:1 dilution of the protein solution with a 500 mM MESNa solution in 1x PBS at 4°C for 1 h. Samples were taken before addition of MESNa, after 0 h and 2 h of cleavage for reaction monitoring. A second Ni-NTA was performed for TRX with the cleaved product. However, eluent B was changed for this purpose to 1x PBS with 250 mM imidazole. The fractions containing the purified TRX were pooled. After that, a dialysis was performed with 50 mM potassium phosphate buffer at pH 7. In the end, the solution was centrifuged at 4 °C and 3,500 rpm for 10 min using a Beckman Coulter Avanti J-26 XP centrifuge. The TRX concentration was measured via Nanodrop 2000c from Thermo Scientific and hence diluted to a concentration of 1 mg/mL. The TRX solution was aliquoted and stored in the freezer at -80 °C.

2.6 Silica particle protein adsorption studies

2.6.1 General protocol for adsorption of eGFP

Adsorption trials were performed employing silica particles precipitated as described in 2.4 as well as eGFP solutions in 50 mM phosphate buffer pH 7 at different concentrations obtained via expression as explained in 2.5. For this a 1 mg/mL eGFP stock solution was diluted to reach the respective concentration. In general, a silica particle stock suspension was vortexed and sonicated for 5 min to obtain a homogenous suspension. This was diluted and the respective amount needed for each experiment was calculated and transferred into an Eppendorf tube, centrifuged at 14,000 rpm for 5 min using an Eppendorf centrifuge 5418 230 V/50-60 Hz. The supernatant was removed and silica particles were suspended in an eGFP solution with a known concentration afterwards and incubated at rt, while shaking at 500 rpm in the dark using an Eppendorf Thermomixer Comfort 5355. After the incubation time, all samples were centrifuged again with the usual settings for supernatant removal. All supernatants were measured and compared to a control fraction using a UV-VIS and FLD detector Dionex 3000 UltiMate HPLC system employing a C4 column, 5-65% of eluent B, 30 min, 1 mL/min or a Biotek Synergy Mx plate reader. The peak area of the eGFP UV trace at 214 nm was used for quantification of the adsorbed fluorescence protein by subtraction of control and supernatant. The peak area 214 nm was determined by manually picking of the peak range. The plate reader results were only used as qualitative measure. During the experiments the following parameter were varied: incubation time, silica particle concentration and eGFP concentration as

further described in 2.6.1.1 to 2.6.1.3. The best conditions which were chosen after these trials are summarized in 2.6.1.4.

2.6.1.1 Optimal eGFP concentration

The eGFP concentration for further adsorption experiments was determined using a steady silica particle concentration of 2.2 mg/mL and four different concentrations of eGFP in 50 mM phosphate buffer. Therefore, 0.5 mg/mL, 0.25 mg/mL, 0.125 mg/mL and 0.0625 mg/mL solutions were prepared by dilution of a 1 mg/mL stock solution. For every single eGFP dilution a control faction was prepared for comparison. This control was not treated with silica particles. The chosen incubation time for this experiment was 3 h.

2.6.1.2 Optimal silica particle concentration

The silica particle concentration providing the highest adsorption percentage was determined using six different concentrations of silica particles. Therefore, 0.5 mg/mL, 1 mg/mL, 2 mg/mL, 3 mg/mL, 4 mg/mL and 5 mg/mL suspensions were prepared by dilution of a 5 mg/mL silica particle stock suspension in 50 mM potassium phosphate buffer at pH 7. The concentration of eGFP was fixed at 0.5 mg/mL for all experiments with an incubation time of 3 h. The best performing silica particle concentration was found after comparing the peak areas obtained for 214 nm of all supernatants after incubation in order to see which approach provided the lowest peak area and hence gave the highest eGFP adsorption.

2.6.1.3 Optimal incubation time

The trials for the best incubation time were performed using eight different incubation times. The best incubation time was defined to be on the one hand as short as possible to decrease down time and allow for more experiments and on the other hand as long as needed to allow for protein adsorption and to see measurable differences between the control and the supernatant after incubation. For this, an eGFP dilution with a concentration of 0.125 mg/mL was prepared using the 1 mg/mL stock solution in 50 mM potassium phosphate buffer at pH 7. Every 15 min, a sample was taken and measured with HPLC up to a total incubation time of 120 min.

2.6.1.4 Adsorption of eGFP using optimized conditions

The experiments for adsorption of eGFP onto silica particles were performed using the optimized conditions previously trialed as explained in 2.6.1.1 to 2.6.1.3. For this, incubation time, eGFP and silica particle concentration were evaluated resulting in the most reasonable silica particle concentration of 4 mg/mL, an eGFP concentration of 0.1 mg/mL and 15 min incubation time for the final approaches. This was done similar to

the general protocol as explained in 2.6.1. The so produced eGFP-silica particles were used to determine whether the eGFP can be released again or not and if it still gives a fluorescence signal after a successful release. A general protocol for the release is given in 2.8.1.

2.6.1.5 Determination of the adsorbed amount of eGFP

The exact way for calculation of the amount of adsorbed eGFP in reference to 2.6.1.4 shall be explained which leads from the obtained UV peak areas to the final eGFP amount adsorbed given in nmol/g silica. The experiment was performed using a total volume of 100 µL, but 80 µL were injected because it was not possible to withdraw the whole supernatant without silica particle in it. The experimental areas for the supernatants obtained after eGFP adsorption and the control factions were adjusted linear to the respective area expected for 100 µL to calculate the total amount of eGFP and silica particle in the approach. For eGFP adsorption calculations a mean value for the control fraction was determined using the obtained peak areas at 214 nm. This was further used for determination of the difference of supernatant and control giving the theoretical peak area of adsorbed eGFP. Since it is known how much eGFP is present in the 0.1 mg/mL control fraction of 100 µL it is possible to calculate the amount of adsorbed eGFP. For a 4 mg/mL silica particle solution, the adsorbed amount of eGFP was calculated using equations 1 to 3. Equation 1 gives the total amount of eGFP in mg which was calculated using the concentration of the control 0.1 mg/mL, the reaction volume of 0.1 mL, the average adjusted area of the control and the area of the adsorbed eGFP.

$$eGFP(mg) = \frac{0.1\,\frac{mg}{mL} * 0.1\,mL}{Area\ 214\,nm\ control\ (mAU*min)} * Area\ 214\,nm\ adsorbed\ eGFP\ (mAU * min)$$

Equation 1

Proceeding from this, the amount of silica particle present in the sample is adjusted to 1 mg with a factor of 2.5 because a 4 mg/mL solution was used in a 100 µL scale (Equation 2).

$$eGFP\left(\frac{mg}{mg}silica\ particle\right) = eGFP(mg) * 2.5 = eGFP(\frac{g}{g}silica\ particle)$$

Equation 2

With equation 3 the dimensions are changed to get a concentration value for eGFP in nmol/g silica particle using the molecular weight of eGFP (27,764 g/mol).

$$eGFP\left(\frac{nmol}{g}silica\ particle\right) = \frac{eGFP(\frac{g}{g}silica\ particle)}{27764\ g/mol} * 10^9$$

Equation 3

2.6.2 Adsorption of TRX

Thioredoxin was adsorbed onto silica particles using the same protocol as it is explained for eGFP in 2.6.1.4. The concentration of TRX for this experiment was set to 0.1 mg/mL while a 4 mg/mL silica particle suspension was used. The activity of TRX adsorbed onto silica particles was measured using the protocol as described in 2.1.5. The 17 µL of TRX solution was changed for this purpose to 80 µL of a silica particle suspension loaded with TRX. Accordingly, the buffer volume was adjusted from 73 µL to 10 µL to maintain a total mixture volume of 100 µL. The silica suspension was homogenized with a pipette right before measurement. A mixture without DTT was used as a blank. The results are shown in 3.5.2.

2.7 Protein adsorption to Cy5-R5 silica particles

2.7.1 Adsorption of eGFP

The adsorption of eGFP onto Cy5-R5 (**6**) silica particles was done similar to the adsorption with silica particles precipitated with **4** as described in 2.6.1.4.

2.8 Protein release from silica particles

2.8.1 Release of eGFP

EGFP release was evaluated using silica particles loaded with eGFP as described in 2.6.1.4. Particles were washed twice with a 50 mM potassium phosphate buffer at pH 7 for 5 min to remove excess eGFP and centrifuged at 14,000 rpm for 5 min with an Eppendorf centrifuge 5418 afterwards. The resulting supernatant was removed and the particles were incubated using a 50 mM phosphate buffer at pH 3, pH 7 or pH 9 at rt while shaking at 500 rpm in the dark for 1 h. The silica particle suspension was then centrifuged at 14,000 rpm for 5 min and the supernatant was removed for further analysis with a Dionex 3000 UltiMate HPLC. The peak areas obtained after HPLC UV/Vis measurement were used for quantification of the released eGFP (Equation 1 to 3). A Biotek Synergy Mx plate reader was employed for supernatant measurement using a 1:8 dilution with a volume of 100 µL.

2.9 Protein release from Cy5-R5 silica particles

2.9.1 Release of eGFP and Cy5-R5

The eGFP and Cy5-R5 (**6**) release was investigated using Cy5-R5 silica particles previously loaded with eGFP as described in 2.7.1. The particles were incubated in 50 mM potassium phosphate buffer at pH 3, pH 7 or pH 9 at rt while shaking at 500 rpm for 1 h. This was done in the dark to avoid bleaching. Afterwards, the silica particle suspension was centrifuged at 14,000 rpm for 5 min. The supernatant was removed for further analysis with HPLC and plate reader. The UV peak area obtained after HPLC measurement was used for eGFP quantification (Equations 1 to 3). This was not done for Cy5-R5 because both the unmodified compound **4** and the Cy5 conjugate **6** eluted in the same peak making it impossible to distinguish them. The proof for a successful Cy5-R5 release was done with plate reader employing the wavelength as seen in table 1.

2.9.2 Release of eGFP and Cy5-R5 from dried particles

Silica particles were precipitated using compound **6** and loaded with eGFP according to 2.7.1. The particles were washed with 50 mM potassium phosphate buffer at pH 7. After that, they were washed three timed with ddH_2O and air dried for 30 min. The particles were incubated in ethanol for 1 h at room temperature and then treated with 50 mM potassium phosphate buffer at either pH 3 or pH 9. The eGFP and Cy5-R5 release was determined using plate reader measurement. The supernatants were diluted 1:2 for measurement. The respective results are analyzed in 3.8.2.

Chapter 3

Results and discussion

3.1 Final analysis of Cys-R5 (R5)

Cys-R5 (R5, **4**) was successfully synthesized with a yield of 27%, referred to the used amount of resin, by manual synthesis as described in 2.2. HPLC analysis of the purified compound (Figure 16A) gave a single sharp peak in both UV channels at 214 nm and 280 nm. MS analysis showed four peaks which correlate with the calculated mass/charge values: m/z = 1059.22 $(M+2H)^{2+}$, m/z = 706.48 $(M+3H)^{3+}$, m/z = 530.11 $(M+4H)^{4+}$and m/z = 424.29 $(M+5H)^{5+}$. The peptide was thus used for Cy5-R5 synthesis as described in 2.3 as well as for silica particle precipitation described in 2.4.

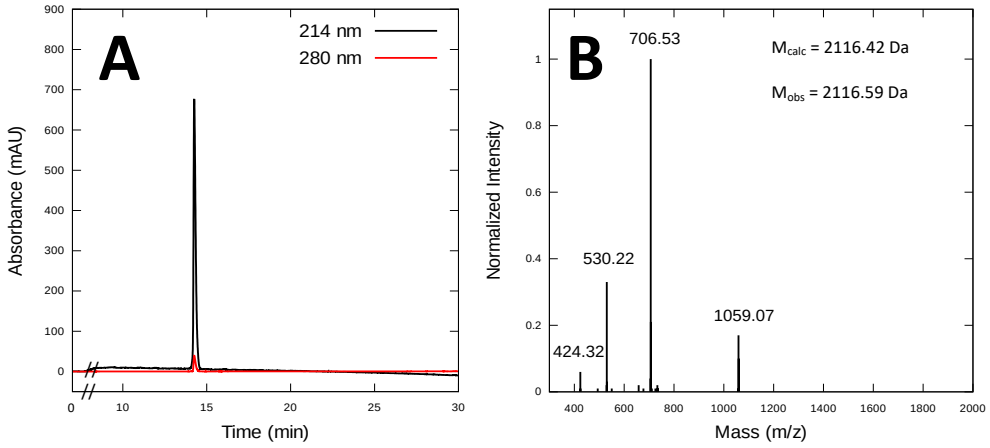

*Figure 16 – Final analysis of **4**; **A**: HPLC chromatogram, C18, 5-65% B, 30 min,1 mL/min, retention time: 14.25 min; **B**: Mass spectroscopy analysis, calculated mass = 2116.42 Da, observed mass = 2116.59: m/z = 1059.07 $(M+2H)^{2+}$, m/z = 706.53 $(M+3H)^{3+}$, m/z = 530.22 $(M+4H)^{4+}$, m/z = 424.32 $(M+5H)^{5+}$.*

3.2 Final analysis of Cy5-R5

Cy5-R5 (**6**) was successfully synthesized manually with an obtained yield of 15% as already described in 2.3. The HPLC analysis (Figure 17A) contained a single peak with tailing in both UV channels at 214 nm and 280 nm after 15.98 min retention time. The mass spectroscopy measurement in Figure 17B showed three dominant peaks which were expected for Cy5-R5 at the calculated mass/charge ratios of m/z = 856.5 $(M+3H)^{3+}$, m/z = 642.6 $(M+4H)^{4+}$and m/z = 514.3 $(M+5H)^{5+}$. No additional byproducts were visible for compound **6** as well.

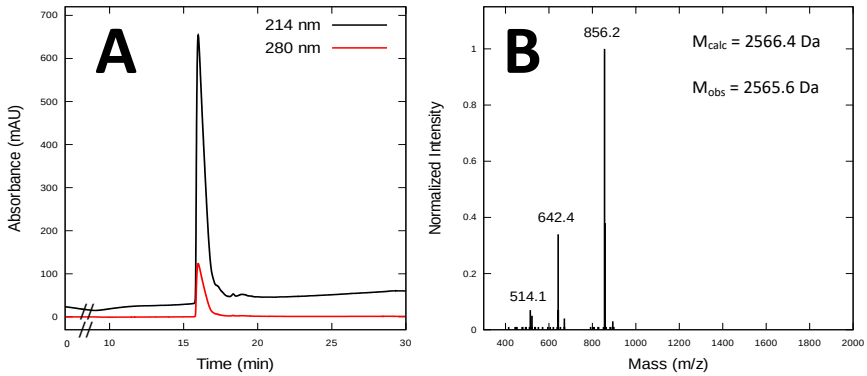

*Figure 17 – Final analysis of Cy5-R5 (**6**); **A**: HPLC chromatogram, C18, 5-65% B, 30 min, 1 mL/min; Retention time: 15.98 min; **B**: Mass spectroscopy analysis, calculated mass = 2566.4 Da, observed mass = 2116.59: m/z = 856.2 $(M+3H)^{3+}$, m/z = 642.4 $(M+4H)^{4+}$, m/z = 514.1 $(M+5H)^{5+}$.*

3.3 Analysis of precipitated silica particles

3.3.1 Silica particles

Precipitation of silica particles using compound **4** was performed as described in 2.4.1. The resulting particles are nearly spherical and aggregated particles are clearly visible in the obtained SEM pictures (Figure 18A and 18B). The surface of the generated silica particles is mainly smooth with a few single exceptions that look like little globules attached on the surface (Figure 18A). The particles' diameter appeared to be in a range between 600 nm and 750 nm. This finding fits well with the diameter of the silica particles obtained by Lechner *et al.*[64]. The particles were further used for eGFP adsorption experiments which are described in 2.6.1 as well as thioredoxin adsorption explained in 2.6.2.

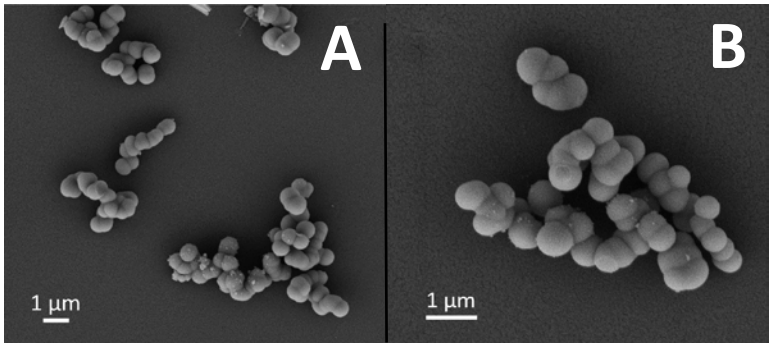

*Figure 18 – SEM images of silica particles using **4**; **A**: Magnification 5000x; **B**: Magnification 10000x.*

3.3.2 Cy5-R5 silica particles

Cy5-R5 silica particles were successfully synthesized using **6** according to the protocol in 2.4.2 and subsequently imaged with SEM (Figures 19A and 19B). The particles exhibit no significant difference in shape or size compared to the silica particles precipitated with **4** (Figures 18A and 18B). However, the number of globules attached to the surface were determined by eye to be decreased in comparison to the particles in Figure 18A. Another difference is that the normal silica particles have a white/grey color whereas the Cy5-R5 silica particles exhibit a strong blue color (Figure 19C) which is due to the attached dye Cy5. The supernatant is blue because the precipitation solution is shown in the picture.

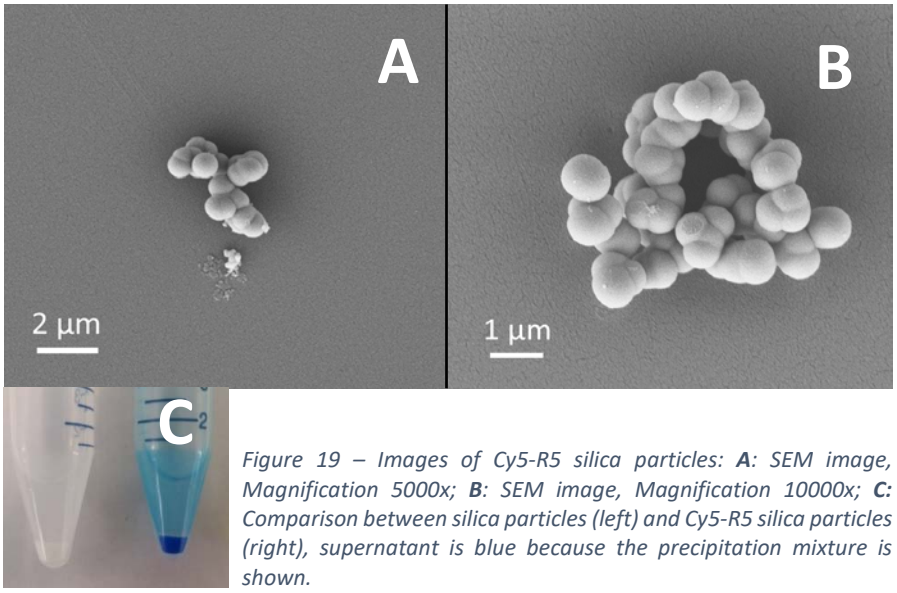

*Figure 19 – Images of Cy5-R5 silica particles: **A**: SEM image, Magnification 5000x; **B**: SEM image, Magnification 10000x; **C:** Comparison between silica particles (left) and Cy5-R5 silica particles (right), supernatant is blue because the precipitation mixture is shown.*

3.3.3 Discussion silica particle precipitation

Kamalov *et al.*[81]. were able to demonstrate that the N-terminal residue of the silaffin peptide R5 is important for the established morphology of the resulting silica particles. They synthesized five different variants of R5 with altered N-terminal residues of which two were further investigated regarding the relation between peptide dimerization and the morphology of the resulting silica particles. For R5 and the modified Cy5-R5, a relation between higher dimerization and smoother surface could be determined[81]. The dimerization was increased through an increase of incubation time of the R5 variant solution before silica precipitation was initiated. The maximum was reached after 8 h of incubation yielding smooth silica particles. That fact that the obtained silica particles in this project (Figure 18A) did show some single globules on the surface after overnight incubation of **4** is in a small contrast to the results obtained by Kamalov *et al.*[81]. This could be due to some contamination which interfered with the dimerization process of **4**.

However, this is unlikely because Figure 16 shows a clean product. For this dimerization process, phosphorylation or at least a phosphate buffer have been found essential[57,82] which was also used in our experiments as described in 2.4.1. Furthermore, R5 contains an N-terminal cysteine which is also able to form covalent dimers via a disulfide with another Cys-R5 peptide. This dimerization facilitates silica precipitation. As the dimerization of cysteine is based on an oxidation reaction in an aqueous solution, a possible contaminant could be any reducing agent which could come into the mixture by accident. Another possible cause is, that the cysteine residue was still protected as a thioether with a trityl residue after peptide synthesis and purification which inhibits the disulfide generation. However, no such peak was visible in the mass spectra for both peptides (Figure 16A and 17A) so it can be excluded.

Lechner *et al.*[64] published in 2015 that they were able to synthesize two R5 variants with attached eGFP and TRX able to generate silica particles out of silicic acid. They showed that it is possible to encapsulate a cargo when attached to R5 during silica precipitation[64]. The experiments in the study on hand were carried out using Cy5 as cargo attached to **4**.

3.4 Protein expression and purification of eGFP and TRX

3.4.1 Expression of eGFP

The enhanced green fluorescent protein was expressed via *E. coli* expression previously described in 2.5. With a molecular weight of 27,764 Da the respective eGFP band was expected around the 30,000 Da marker band. The observed band of eGFP can be seen at t=4 h and is not visible before addition of IPTG at t=0 h expression time (Figure 20A). This indicates a successful initiation of eGFP expression. Other bands are related to cell products which were not analyzed further. The Ni-NTA fractions 28 to 44 contained eGFP in an adequate purity (Figure 20B) while the respective mainpool yielded eGFP in a high purity (Figure 20C). The chromatogram (Figure 21) confirmed that by showing a single peak at 19.2 min retention time. The successfully expressed eGFP was used for the eGFP adsorption experiments as described in 2.6.1 and 2.7.1.

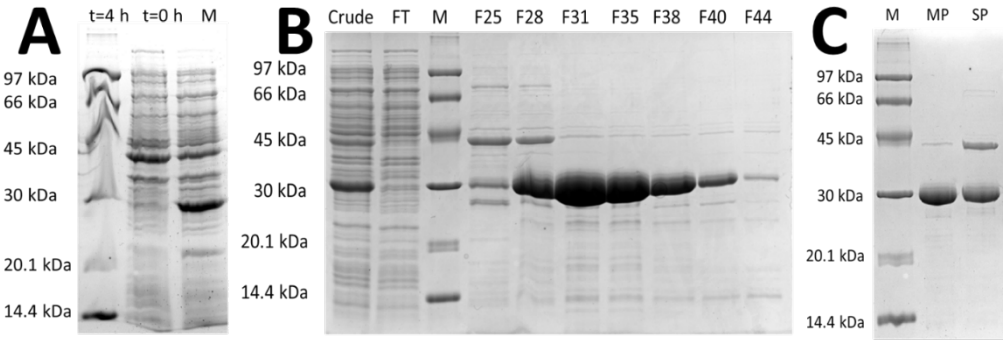

*Figure 20 – Expression and purification of eGFP; **A**: Expression eGFP, M_{eGFP} = 27764 Da (245 aa, Protparam); left to right: Expression time t=4 h, t=0 h, Marker; **B**: Fractions after Ni-NTA purification, left to right: Crude, eGFP, Flowthrough (FT), Marker (M), Fractions 25, 28, 31, 35, 38, 40 and 44; **C**: Final analysis of eGFP, left to right: Marker (M), main pool (MP), side pool (SP).*

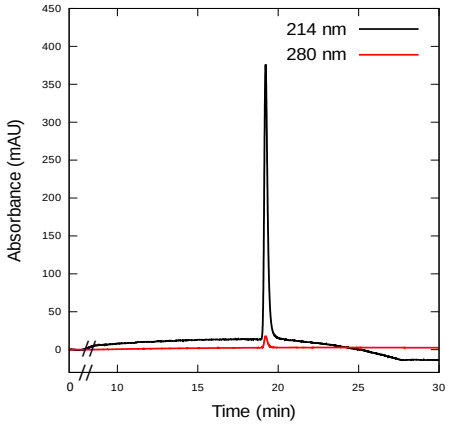

Figure 21 - Final analysis of eGFP, HPLC chromatogram, C4, 5-65 % B, 30 min, 1 mL/min; Retention time: 19.2 min.

3.4.2 Expression of TRX

Expression of TRX was performed as described in 2.5. A product band after 2 h expression time can be seen around 42,000 Da which marks the TRX full-length construct (Trx-Intein-CBD) and its successful expression with the utilized method. The full-length construct is the expressed protein prior to MESNa cleavage. Both the supernatant and the pellet contained TRX, but the supernatant in higher purity (Figure 22A). The fractions obtained after the first Ni-NTA contained the TRX full-length construct from fraction 13 to 21 (Figure 22B). Additionally, a precleavage took place according to the bands at around 28,000 Da (Intein product). During MESNa cleavage, the bands for the intein product and TRX (12,700 DA) increased in intensity (Figure 23A). The second Ni-NTA yielded the full-length construct in factions 24 to 31 and the purified TRX in fractions 10 to 13 (Figure 23B). The TRX band is the only visible band in the final analysis gel which implies a high purity (Figure 23C). The respective chromatogram confirmed that by

showing one peak for TRX (Figure 24A). The activity measurement proved that TRX stayed active during the expression and purification steps (Figure 24B). The absorbance increases over time in a sigmoid function due to the precipitation of the insulin B chain. A sigmoidal behavior was expected for enzyme activity. Altogether, the expression of TRX was a success and it was further used for adsorption trials as described in 2.6.2.

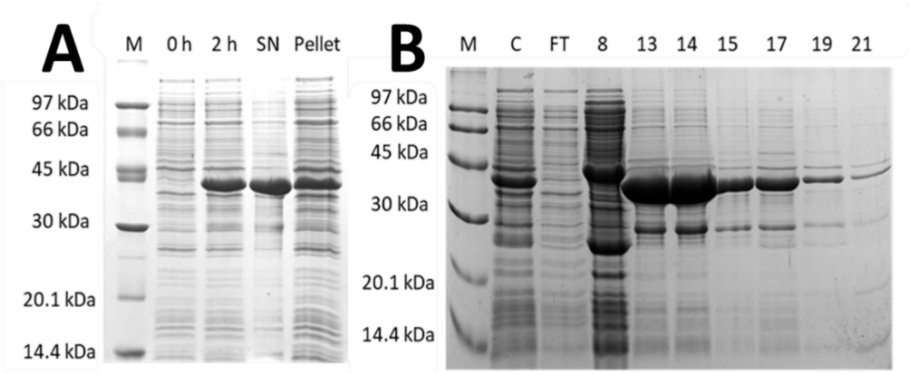

*Figure 22 – Thioredoxin expression and first purification with Ni-NTA, TRX full length construct "42" kDa; **A**: Expression and cell disruption gel, left to right: Marker (M), 0 h expression time, 2 h expression time, supernatant (SN) and pellet after cell disruption; **B**: First Ni-NTA purification, left to right: Marker (M), crude (C), flowthrough (FT), fractions 8, 13, 14, 15, 17, 19 and 21.*

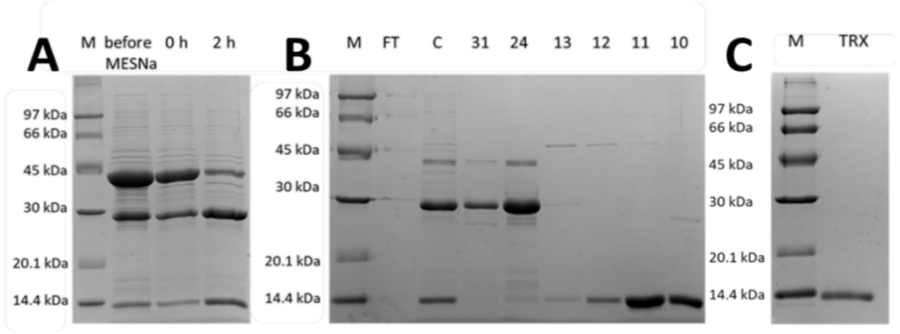

*Figure 23 - MESNa cleavage, second Ni-NTA purification and final analysis SDS-gels of thioredoxin; **A**: 250 mM MESNa cleavage, left to right: Marker (M), before addition of MESNa, 0 h and 2 h cleavage time; **B**: Second Ni-NTA purification, left to right: Marker (M), Flowthrough (FT), Crude (C), Fractions 31, 24, 13, 12, 11 and 10; **C**: TRX final analysis, left to right: Marker (M), pure TRX.*

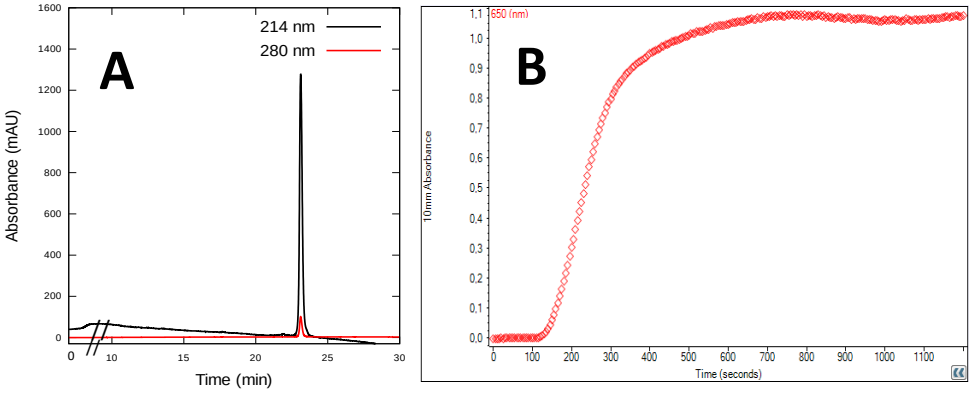

*Figure 24 – Final analysis of TRX; **A**: Chromatogram (HPLC), C18 column, 5-65 % B, 30 min,1 mL/min, Retention time: 23.1 min; **B:** Activity measurement of TRX (10µM) using insulin, turbidity measurement at 650 nm.*

3.5 Silica particle adsorption studies

3.5.1 Adsorption of eGFP

Adsorption of eGFP onto the surface of silica particles was achieved through passive diffusion by incubation of the particles in an eGFP solution. For this, the optimal silica particle and eGFP concentration as well as incubation time were determined.

3.5.1.1 Optimal eGFP concentration

For evaluation of the optimal eGFP concentration a detailed description is given in 2.6.1.1. The comparison of the obtained supernatants can be seen in Table 12 with the respective calculated percentage of adsorbed eGFP. The optimal eGFP concentration was defined to have the highest percentual difference between supernatant and control after incubation and hence the highest percent of adsorbed eGFP. This was intended to simplify manual interpretation and analysis of the HPLC peaks at 214 nm.

Table 12 - Results for eGFP adsorption for different eGFP concentrations, 2.2 mg/mL silica particle, HPLC injection volume 20µL, chosen concentration 0.125 mg/mL is highlighted in green; experiment was performed with one sample each.

Sample label	c [eGFP] (mg/mL)	Area 214 nm (mAU*min)		% adsorbed
		Supernatant	Control	
A	0.5	151.79	165.54	8.31
B	0.25	74.51	76.40	2.47
C	0.125	34.08	42.43	19.68
D	0.0625	13.64	18.56	26.51

The adsorbed percentage increases with a lower eGFP concentration (Table 12). This was expected because the adsorbed amount of eGFP is assumed to be similar for every approach, while the provided amount of eGFP decreased. This could be because the size of inner and outer surface as well as pore diameter and pore volume are important for the adsorbed amount of protein[36,41]. Sample A and B stand in contrast to this assumption: while having a higher eGFP concentration, the adsorbed percentage for sample A is higher when compared with sample B. Sample D (0.0625 mg/mL eGFP) displayed the highest percentage for eGFP adsorption with 26.51% when comparing the peak area at 214 nm of the supernatant with the control. However, the concentration of sample C (0.125 mg/mL eGFP) with 19.68% adsorbed eGFP was chosen for further experiments because of its higher total peak area (214 nm) compared with sample D as well as the higher difference between control and supernatant. For easy dilution, the chosen concentration was altered to 0.1 g/mL eGFP in 50 mM potassium phosphate buffer.

3.5.1.2 Optimal silica particle concentration

In 2.6.1.2 the protocol for evaluation of the optimal silica particle concentration is specified. For this, one sample for each concentration was prepared and analyzed. The results in table 13 show the employed silica particle concentration with the peak area at 214 nm of the obtained supernatants. A lower peak area indicates, that less eGFP is present in the supernatant and hence more eGFP was adsorbed onto silica particles. A higher silica particle concentration was expected to give a lower peak area due to the increased surface which can adsorb more eGFP when compared to lower silica particle concentrations. The peak areas obtained in our experiment decreased from 167.46 mAU*min for 0.5 mg/mL silica particle to 159.07 mAU*min for 5 mg/mL silica particle. However, samples B and E appeared to be an exception as the peak area value was increased when compared to the next lower concentration. Furthermore, for eGFP supernatants treated with silica particle concentrations greater or equal 3 mg/mL no longer decreased but remained nearly constant. Hence, the concentration of 4 mg/mL silica particle was chosen for future adsorption experiments (Table 13, green). Nevertheless, it is noticeable that the peak area differs 5 % between sample A and F. This was not intuitive because one would expect a higher decrease of the peak area for a tenfold higher silica particle concentration having an increased surface size for additional adsorption. This could probably be due to a mistake made during this experiment such as an ineffective homogenization of the suspension during incubation.

Table 13 - Results for silica particle concentration trials performed with one sample for each concentration, injection volume 20µL, 0.5 mg/mL eGFP chosen silica particle concentration is highlighted in green; experiment was performed with one sample each.

Sample label	c silica particle (mg/mL)	Area supernatant 214 nm (mAU*min)
A	5	159.07
B	4	158.07
C	3	159.44
D	2	169.64
E	1	175.35
F	0.5	167.46

3.5.1.3 Optimal incubation time

The best incubation time was found considering both the lowest peak area for the supernatant and a practical incubation time. For this, one sample for each incubation time was prepared and analyzed. The results show that a high amount of eGFP was already adsorbed after 15 min incubation time with a peak area of 115.78 mAU*min compared to the control with 161.55 mAU*min (Table 14). Up to 120 min the area value decreases further to 92.50 mAU*min. The peak area value after 60 min incubation time was determined to 113.20 mAU*min. In reference to the other obtained results this value seems to be an exception as it is higher as the value after 45 min incubation time (110.35 mAU*min). When comparing the values from the highest to the lowest peak area, it can be seen that the areas usually decrease by ~ 2-4 mAU*min. However, another exception appeared after 120 min of incubation time with 92.50 mAU*min which is decreased by ~13 mAU*min compared to the value for 105 min incubation time. It was decided that the adsorbed amount after 15 min is sufficient in order to perform as many measurements as possible in less time.

Table 14 - Results for incubation time trials performed with one sample for each incubation time, 80 µL injection volume for HPLC, 4 mg/mL silica particle, 0.125 mg/ml eGFP, chosen incubation time is highlighted in green; experiment was performed with one sample each.

Incubation time (min)	Area 214 nm eGFP (mAU*min)
control	161.55
15	115.78
30	112.10
45	110.35
60	113.20
75	109.79
90	107.89
105	105.40
120	92.50

3.5.1.4 Adsorption of eGFP using optimized conditions

As previously mentioned in 2.6.1.4, silica particles were loaded with eGFP using the optimized conditions trialed in 2.6.1.1 to 2.6.1.3. The respective results are analyzed in 3.5.1.1 to 3.5.1.3. The areas of all nine measured supernatants are decreased after eGFP adsorption compared to the control (Table 15). This indicates, that eGFP was successfully adsorbed onto the silica particles during incubation.

Table 15 - Obtained peak areas for silica particle eGFP adsorption using 0.1 mg/mL eGFP, 4 g/mL silica particles and 15 min incubation time; Experimental area 214 nm obtained with HPLC. injection volume 80 µL; Adjusted/calculated area for 100 µL injection volume.

Sample	Experimental area 214 nm (mAU*min); V=80 µL	Average±Error (V=100 µL) (mAU*min)	Calculated area 214 nm (mAU*min); V= 100 µL	Average±Error (V=100 µL) (mAU*min)
Control 1	101.17	107.23±4.32	126.47	134.04±5.40
Control 2	109.56		136.95	
Control 3	110.96		138.69	
SN 1	75.56	77.35±1.81	94.44	96.68±2.26
SN 2	75.26		94.07	
SN 3	78.75		98.44	
SN 4	76.43		95.53	
SN 5	77.10		96.38	
SN 6	76.18		95.23	
SN 7	81.18		101.47	
SN 8	78.93		98.67	
SN 9	76.72		95.90	

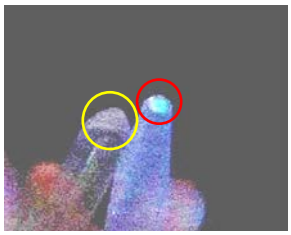

Figure 25 – Eppendorf tubes with silica particles in UV light: without (left, yellow) and with eGFP (right, red)

Furthermore, we were able to show the adsorption of eGFP by applying UV light (Figure 25). On the left, silica particles without eGFP did not respond with fluorescence but the eGFP treated silica particles on the right emitted a clearly visible fluorescence. It was not validated whether eGFP also absorbed into the silica particles, but considering their porous structure it is assumable. The chromatogram (Figure 26C) visualized this adsorption: The black peak, showing the control faction with a retention time of 17.6 min, is higher and bigger compared to the supernatant peak displayed in red. Another peak visible in the supernatant at a retention time of 11.2 min most probably refers to compound **4** which was passively washed out. However, this fraction was not collected and not analyzed further. For eGFP, the retention time was different compared to the final analysis with 19.2 min (Figure 21). The incubation with compound **4** may have some influence on this but it was not investigated further. The data in Table 16 proves that eGFP was successfully loaded onto silica particles with an average concentration of 250.95 ± 15.18 nmol/g silica which was calculated using equations 1 to 3. Additionally, SEM images of the eGFP loaded silica particles were taken (Figure 26A and B). There is no significant change in the appearance when compared to the untreated silica particles in Figure 18.

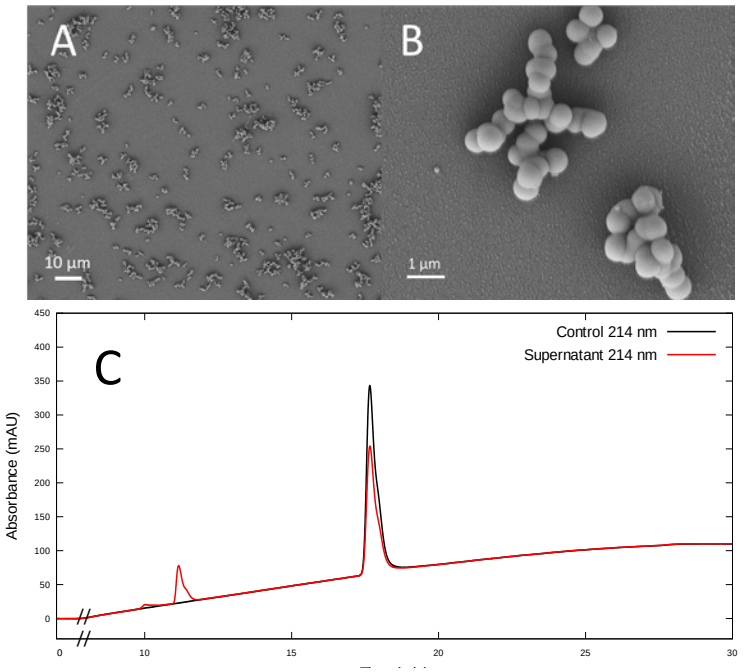

*Figure 26 - SEM images of eGFP loaded silica particles and HPLC chromatogram, **A**: SEM image, magnification 500x; **B**: SEM image, magnification 10000x; **C**: - HPLC chromatogram (C4 column, 5-65 % B, 30 min, 1 mL/min) of 0.1 mg/mL eGFP control and respective supernatant after silica particle incubation; Black: Control 214 nm, Red: Supernatant 214 nm; Retention time: R5: 11.2 min eGFP:17.6 min.*

Table 16 - Adsorbed eGFP amount using silica particles, Area 214 nm of adsorbed eGFP was calculated by subtraction of the supernatant and the control, eGFP concentration was calculated as described with equations 1 to 3.

	Area 214 nm of adsorbed eGFP(mAU*min)	**[EGFP] (nmol/g silica)**
Control – SN1	39.59	265.98
Control – SN2	39.97	268.48
Control – SN3	35.60	239.15
Control – SN4	38.50	258.66
Control – SN5	37.66	253.00
Control – SN6	38.81	260.71
Control – SN7	32.56	218.75
Control – SN8	35.37	237.61
Control – SN9	38.14	256.19
Average±Error	37.35±2.26	250.95±15.18

3.5.2 Adsorption of TRX

Adsorption experiments using TRX were performed according to the protocol for eGFP described in 2.6.2. The obtained peak areas with the respective adjusted values for TRX control and supernatant can be seen in table 17. After performing the calculations using equation 1 to 3 and the average control value of 80.17 mAU*min, it was determined that a total of 572.63 ± 206.20 nmol TRX/g silica were adsorbed using silica particles (Table 17). The high standard deviation results from the SN1 value which seems to be an exception. If it is not considered during calculations, a total of 427.85 ± 29.92 nmol TRX/g silica was adsorbed. The concentration of TRX is nearly doubled compared to the adsorbed amount of eGFP (Figure 27). This could probably be due to the different molecular weight of both cargos. While eGFP has a molecular weight of 27,764 Da, TRX has a molecular weight of 12,712 Da. Having TRX weighing half the amount of eGFP it is reasonable that more molecules of TRX can be adsorbed onto silica particles when compared to eGFP. The activity measurement of TRX using TRX loaded silica particles was not successful. Prior to measurement, the silica suspension was homogenized. This resulted in a high turbidity measured at 650 nm at the beginning of the experiment. This was not expected because the activity measurement in Figure 24B showed, that the turbidity should have been low instead. During the experiment, the turbidity decreased which could probably come from the settlement of the silica particles in the suspension. It was not possible to obtain an increase for turbidity during the performed experiments. However, this does not give any information whether TRX was accessible and active while adsorbed onto the silica particles or not. It can be possible that the decrease in turbidity during the slow settlement of silica particles completely covered the increase of turbidity from active TRX. To verify this theory, activity measurement could be conducted with a longer monitoring period to see if the turbidity increases again or lies higher then seen in Figure 24B after all silica particles are settled.

Table 17 - Obtained peak areas for silica particle TRX adsorption using 0.1 mg/mL TRX, 4 g/mL silica particles and 15 min incubation time; Experimental area 214 nm obtained with HPLC. injection volume 80 µL; Adjusted/calculated area for 100 µL injection volume.

Sample	$Area_{exp}$ 214 nm (mAU*min), V=80 µL	$Area_{Calc}$ 214 nm (mAU*min), V=100 µL	Area 214 nm of adsorbed TRX (mAU*min)	C [TRX] (nmol/g silica)
Control 1	58.02	72.52	-	-
Control 2	67.44	84.30	-	-
Control 3	66.95	83.69	-	-
Average ± Error	64.14 ± 4.33	80.17 ± 5.41	-	-

Sample	$Area_{exp}$ 214 nm (mAU*min), V=80 µL	$Area_{Calc}$ 214 nm (mAU*min), V=100 µL	Area 214 nm of adsorbed TRX (mAU*min)	C [TRX] (nmol/g silica)
SN 1	36.02	45.02	35.15	862.19
SN 2	49.21	61.51	18.66	457.77
SN 3	51.16	63.95	16.22	397.93
Average ± Error (SN1 to SN3)	45.46 ± 6.72	56.83 ± 8.41	23.34 ± 8.41	572.63 ± 206.20
Average ± Error (SN2 & SN3)	50.18 ± 0.98	62.73 ± 1.22	17.44 ± 1.22	427.85 ± 29.92

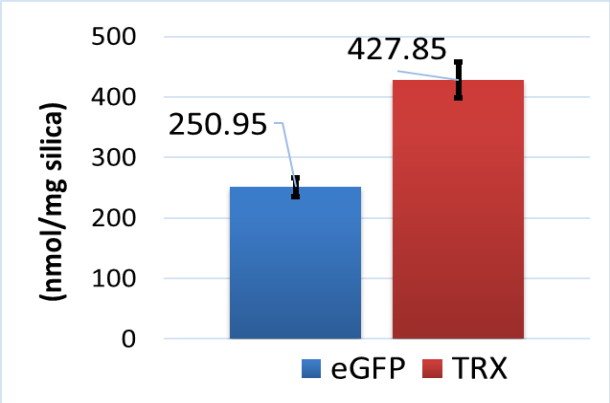

Figure 27 – Comparison of adsorbed amount of eGFP (M_W= 27,764 Da, blue) and TRX (M_W= 12,712 Da, red) using silica particles.

3.6 Adsorption studies with Cy5-R5 silica particles

3.6.1 Adsorption of eGFP

Adsorption experiments using eGFP and Cy5-R5 generated silica particle were performed following the protocol described in chapter 2.7.1. The particles were precipitated according to the general procedure as specified in chapter 2.4. In table 18 the determined areas of the eGFP peak in mAU*min are listed which appeared to be in a similar scale compared to the data in Table 15. After performing the calculations using equations 1 to 3 and determining the average of the results in table 18, it was specified that a total of 272.21 ± 9.12 nmol eGFP/g silica were adsorbed using Cy5-R5 silica particles (Table 19). The Cy5-R5 silica particles adsorbed a similar amount of eGFP when compared to the normal silica particles (see Figure 28A). The difference lies within the error ranges and is

thus not significant. Their appearance by eye of the silica particle was not altered after the eGFP load (Figure 28B).

Table 18 - Obtained peak areas for Cy5-R5 silica particle eGFP adsorption using 0.1 mg/mL eGFP, 4 g/mL silica particles and 15 min incubation time; Experimental area 214 nm obtained with HPLC. injection volume 80 µL; Adjusted/calculated area for 100 µL injection volume.

Sample	$Area_{exp}$ 214 nm (mAU*min), V=80 µL	Average ± Error, V=80 µL (mAU*min)	$Area_{Calc}$ 214 nm (mAU*min), V=100 µL	Average ± Error, V=100 µL (mAU*min)
Control 1	99.32	105.50 ± 4.38	124.16	131.87 ± 5.47
Control 2	108.15		135.19	
Control 3	109.01		136.27	
SN 1	72.84	73.60 ± 1.07	91.04	92.01 ± 1.34
SN 2	73.44		91.80	
SN 3	74.96		93.70	
SN 4	73.87		92.33	
SN 5	72.42		90.52	
SN 6	74.84		93.55	
SN 7	72.19		90.23	
SN 8	72.81		91.02	
SN 9	75.08		93.85	

Table 19 - Adsorbed eGFP amount using Cy5-R5 silica particles, Area 214 nm of adsorbed eGFP was calculated by subtraction of the supernatant and the control, EGFP concentration was calculated as described with equations 1 to 3.

Sample	Area 214 nm of adsorbed eGFP (mAU*min)	C [EGFP] (nmol/g silica)
Control – SN1	40.83	278.78
Control – SN2	40.07	273.63
Control – SN3	38.17	260.67
Control – SN4	39.54	269.97
Control – SN5	41.35	282.33
Control – SN6	38.32	261.64
Control – SN7	41.64	284.32
Control – SN8	40.85	278.96
Control – SN9	38.02	259.62
Average ± Error	39.87 ± 1.34	272.21 ± 9.12

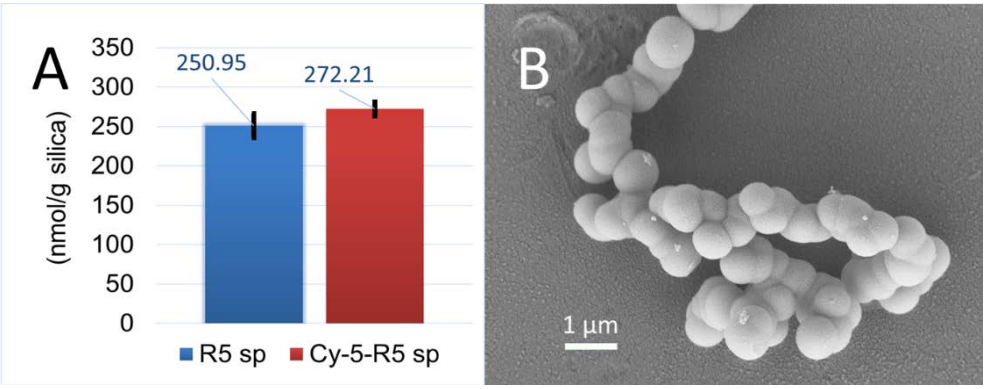

*Figure 28 – Results eGFP adsorption; **A**: Comparison of eGFP adsorption using silica particles (blue) and Cy5-R5 silica particles (red); no significant difference was observed for eGFP adsorption behavior of both particle types; **B**: SEM image 10k magnification of eGFP loaded Cy5-R5 silica particles; sp=silica particles*

3.7 Discussion of silica and Cy5-R5 silica particle adsorption studies

The different amount of adsorbed protein for eGFP and TRX could be due to the difference in size, molecular weight and surface area of both proteins as well as due to different interaction strength or mechanisms with the silica surface. EGFP has a molecular weight of 27,764 Da whereas TRX has a molecular weight of 12,712 Da. Although pore size and pore size distribution for R5 silica were not determined in the course of this study, it might have an influence on the adsorption behavior because a smaller protein could fit better in the pores of the silica particles than a bigger protein. Therefore, eGFP or TRX uptake by adsorption could possibly be increased further if the pore diameters for R5 silica would be increased[83,84]. Silica materials with a very large pore diameters are known, e.g. the Santa Barbara Amorphous batch 15 (SBA-15) with pore diameters of 30 nm reported in 1998 by Zhao *et al*.[85]. Pore diameters >6nm can be achieved by addition of copolymer surfactants such as P123 or CTAB[86,87]. The reaction temperatures for this can range from 80°C to 125°C[83]. Such temperatures cannot be employed for R5 silica particles because that would likely destroy the precipitating peptide R5. When looking at the surface area of both proteins a similar difference compared to the molecular weight can be observed. For interpretation, model variants of both proteins were chosen having a similar amino acid sequence as well as molecular weight. While the eGFP variant 5N9O has a surface area of 34,257.598 Å^2, the TRX 1ERT variant's surface area is mere 12,204.771 Å^2. Surface areas for both proteins were calculated based on the protein data base (PDB) using PyMol. EGFP has a surface area nearly three times larger than TRX. The surface area of a protein gives information about the area accessible to a solvent. However, for our experiment it can give an idea that eGFP has a bigger surface occupying more of the accessible space of the silica particle surface when compared to TRX. Furthermore, a

larger surface could provide more options for a stronger and more successful interaction with the particle surface thus resulting in a higher adsorption of eGFP. This needs to be investigated further to verify if this is the case for the employed proteins. It is known, that the adsorption of a protein onto mesoporous silica does not only depend on the employed silica but also on size and properties of the respective protein[64]. It was not determined in our study on which protein-silica surface interactions the adsorption is based on for both eGFP and TRX. Nevertheless, it is of high importance to understand that interaction in order to increase protein adsorption further. According to ProtParam, the pI of GFP (P42212) is 5.67 and the pI of TRX (P0AA25) is 4.67. At pH 7, when adsorption was observed, the overall charge of both proteins was thus negative. Nothing is known so far about the pka of R5 generated silica making it impossible to predict the condition of the silanol groups at pH 7. As both proteins were negatively charged during adsorption experiments the work of Kubiak-Ossowska *et al*.[88,89] could be of interest. They used bovine serum albumin (BSA) with a pI of 5.1 to study the adsorption of negatively charged proteins to negatively charged surfaces such as silica using fully atomistic molecular dynamics simulations. They were able to demonstrate that BSA is able to adsorb onto negatively charged silica at pH 7 with positively charged subdomain IIIB. The resulting interaction is stable because lysine residues can function as anchors. If the orientation of BSA is not favored and a negatively charged domain faces the silica surface, the protein is able to desorb again[88]. This means that proteins with an overall negative charge are able to adsorb to a negative surface if they have subdomains which are positively charged. It could be worth to consider for future experiments what domains or subdomain exist in the employed protein which shall be adsorbed onto silica and which charges they bear. For GFP, Umakoshi *et al.*[90] found out in 2009 that there are 11 structural domains of which five each have a positive or negative net charge while one has a neutral charge at pH 7. At pH 4, the net charge of nine domains is positive and of two domains is neutral[90]. This could explain why eGFP is not released at pH 3 because the positive charged domains might interact with the silanol groups.

Meissner *et al*.[91] studied the influence of pH as well as ionic strength on protein adsorption onto silica nanoparticles (Ludox TMA type). They investigated lysozyme and β-lactoglobulin in a pH range of 2 to 11. For β-lactoglobulin, having a similar pI to eGFP (pI~5), they found that the maximum amount of protein was adsorbed around pH=4 while no adsorption was found at pH 7 without addition of salt. In the presence of 100 mM NaCl, the adsorption at pH 7 could be increased. The authors assume that this is due to electrostatic and non-electrostatic interactions[91]. In our work, adsorption experiments of eGFP and R5 silica were carried out at pH 7 with 50 mM potassium phosphate buffer which influences adsorption as well. However, Meissner *et al*.[91] used a different kind of silica material with a diameter of 21 nm that has different properties when compared to R5 silica with a particle diameter more than 20 times bigger. Nevertheless, based on the finding of Meissner *et al*.[91] it can be of interest to repeat eGFP adsorption using R5 silica at lower pH values (pH 4) in the absence of salt to see if it is possible to increase the adsorbed amount further. However, the stability or integrity of eGFP at pH 4 has to be considered as well as its solubility in absence of salt.

EGFP adsorption was also investigated by Ma *et al*.[92] in 2010 who used three different kinds of silica nanochannels: MCM-41, SBA-15 and ASNCs (Arrays of silica nanochannels) with pore diameters between 3nm and 8 nm. Due to its negative charge at pH 7.4, the silica surface was functionalized with APTES in THF to increase adsorption. The functionalization with APTES generates positive charges at the silica surface which can interact with the negatively charged eGFP. Unlike 50 mM potassium phosphate buffer they used a mixture of eGFP in water and ethanol (6:4) and incubated the silica particles for 24 h. After that, they measured the volume and concentration of eGFP in the supernatant before and after incubation via UV/Vis measurement at 488 nm[92]. Ma *et al*.[92] determined the amount of adsorbed eGFP for MCM-41 silica to be 8.9 nmol/mg and for ACNCs to be 2.7 nmol/mg of which 7.8 nmol/mg and 2.2 nmol/mg was adsorbed onto the inner surface. MCM-41 does have a higher pore diameter compared to ACNCs probably resulting in a higher adsorption of eGFP inside the particle. They also took fluorescence images and found that the protein was intact after adsorption to the silica surface[92]. In comparison to our finding of eGFP adsorption onto R5 silica particles, Ma *et al*.[92] were able to achieve a higher eGFP adsorption with their employed silica. This could possibly be due to favoring reaction conditions such as ethanol/water vs. 50 mM potassium phosphate buffer or APTES functionalization vs. no APTES while employing an increased incubation time of 24 h vs. 15 min. Additionally, a larger pore size or increased particle surface of MCM-41 could increase eGFP adsorption when compared to R5 silica. However, having R5 inside the silica particles employed for our experiments, adsorption could also be influenced by R5 competing with protein adsorption. For future work, eGFP adsorption could be repeated after functionalization of R5 silica with APTES. This could increase eGFP adsorption as APTES generates positive charges at the silica surface that could interact with the negatively charged eGFP at pH 7.

The adsorption of TRX was successful in reference to the measured supernatants but the activity assay gave no positive result because the measured turbidity at 650 nm was decreasing. However, an increase would have been expected due to precipitation of the insulin β-chain as a result of insulin cleavage by active TRX. After expression, TRX was proved to be active (Figure 24) using the same method as it was employed for TRX loaded silica. No agents were added to the solution which could have a negative impact on enzyme activity. To make sure that no enzyme is degraded during incubation with silica particles prior to measurement it could be helpful to add protease inhibitors for future experiments. Another possible cause could be on the one hand a limited access of TRX inside silica which means that insulin never reached the enzyme and on the other hand the way TRX adsorbed onto the silica surface. The loss in activity could be also due to the loss of the active center facing the silica particle during adsorption making it inaccessible. However, the same method was also carried out by Lechner *et al*.[64] to measure TRX activity of immobilized TRX using R5 silica particles. Lechner *et al*.[64] covalently attached TRX to silaffin peptide R5 and performed a silica precipitation using this variant. TRX was found to be active while bound to R5 and encapsulated into silica. However, the precipitation of the insulin β-chain was delayed compared to free TRX which was probably due to diffusion of DTT[64]. It could be worth to consider if the insulin β-chain is also adsorbed by the silica particles thus decreasing turbidity. However, this was not

investigated during our experiments or the experiments performed by Lechner *et al*[64] and could be an interesting approach for future experiments. During our experiment, the decrease of the turbidity could be related to the settlement of the silica particle in suspension which was homogenized prior to measurement. Even after a time of decrease, the turbidity remained constant and did not change further. We could not demonstrate, that TRX adsorbed to silica particles is still able to actively cleave the insulin molecule. For future experiments, the same method can be tested without homogenization of the suspension.

3.8 Protein release from silica particles

3.8.1 Release of eGFP

The release properties of eGFP loaded silica particles were investigated as specified in 2.8.1. The results for the obtained peak areas at 214 nm show, that the amount of released eGFP increases with increasing pH value (Table 20). In reference to equations 1 to 3, 4.41 ± 0.84 nmol/g silica particle eGFP was released at pH 3, 10.55 ± 0.94 nmol/g silica particles at pH 7 and 68.72 ± 2.54 nmol/g silica particles using the pH 9 buffer (Table 21, Figure 29A). This indicates that higher pH values in the basic area are needed to release eGFP. As 250.95 ± 15.18 nmol eGFP /g silica were adsorbed according to the results in 3.5.1.4, approximately 27% of that were released after 1 h of incubation. The released eGFP is at least partial an active fluorescent protein after loading and release because it stills shows fluorescence when measuring the supernatant with plate reader (Figure 29B). The fluorescence results confirm the results obtained with HPLC as they show the same pH dependent release behavior of eGFP. The HPLC peaks are plotted in Figure 30 with the eGFP peak at a retention time of 17.9 min. In the chromatogram one can also notice that a certain amount of compound **4** is released at pH 3 and a smaller amount at pH 7 while at pH 9 no peak for compound **4** is visible at a retention time of 11.4 min. The amount of released compound **4** was not determined further.

Table 20 – Release results for eGFP using silica particles; 50 mM phosphate buffer at pH 3, pH 7 or pH 9, incubation time 1 h, 4 mg/mL silica particle concentration; Experimental area 214 nm obtained with HPLC, injection volume 80 µL; Adjusted/calculated area for 100 µL injection volume.

Sample	Experimental area 214 nm (mAU*min), V=80 µL	Average ± Error, V=80 µL (mAU*min)	Calculated area 214 nm (mAU*min) V= 100 µL	Average ± Error, V=80 µL (mAU*min)
Control 1	101.17	107.23±4.32	126.47	134.04±5.40
Control 2	109.56		136.95	
Control 3	110.96		138.69	
pH 3 A	0.48	0.52±0.10	0.60	0.66±0.12
pH 3 B	0.43		0.54	
pH 3 C	0.66		0.83	
pH 7 A	1.11	1.25±0.11	1.39	1.57±0.14
pH 7 B	1.27		1.59	
pH 7 C	1.38		1.73	
pH 9 A	7.92	8.18±0.30	9.91	10.23±0.38
pH 9 B	8.61		10.76	
pH 9 C	8.02		10.02	

*Table 21 – Release results for eGFP using silica particles; 50 mM phosphate buffer at pH 3, pH 7 or pH 9, incubation time 1 h, 4 mg/mL silica particle concentration; Calculated area 214 nm (mAU*min) V= 100 µL as seen in table 20 used for calculation according to equations 1 to 3.*

Sample	C [EGFP] (nmol/g silica)	Average ± Error (nmol/g silica)
pH 3 A	4.03	4.41±0.84
pH 3 B	3.63	
pH 3 C	5.58	
pH 7 A	9.34	10.55±0.94
pH 7 B	10.68	
pH 7 C	11.62	
pH 9 A	66.57	68.72±2.54
pH 9 B	72.28	
pH 9 C	67.31	

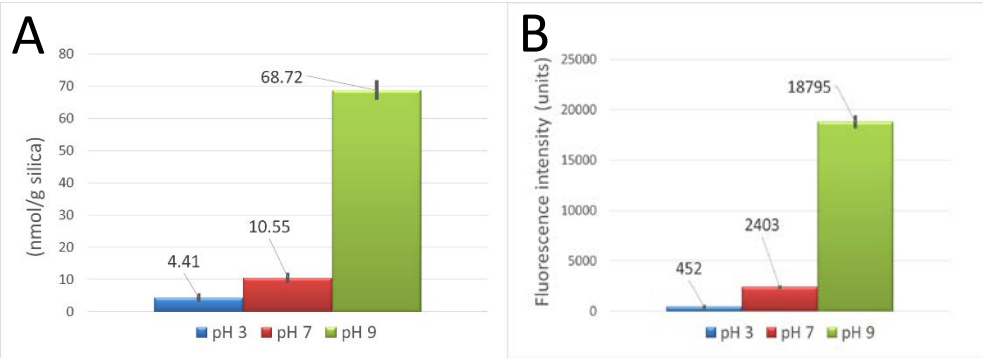

*Figure 29 – Released eGFP using silica particles (4 mg/mL) and 50 mM potassium phosphate buffer at pH 3, pH 7 and pH 9; incubation time 1 h **A**: Calculated amount of released eGFP in nmol/g silica, calculated using the obtained HPLC peaks areas (Table 12); **B**: Relative amount of eGFP released, measurement of the1:8 diluted supernatants (100µL), Excitation: 395 nm, Emission: 509 nm.*

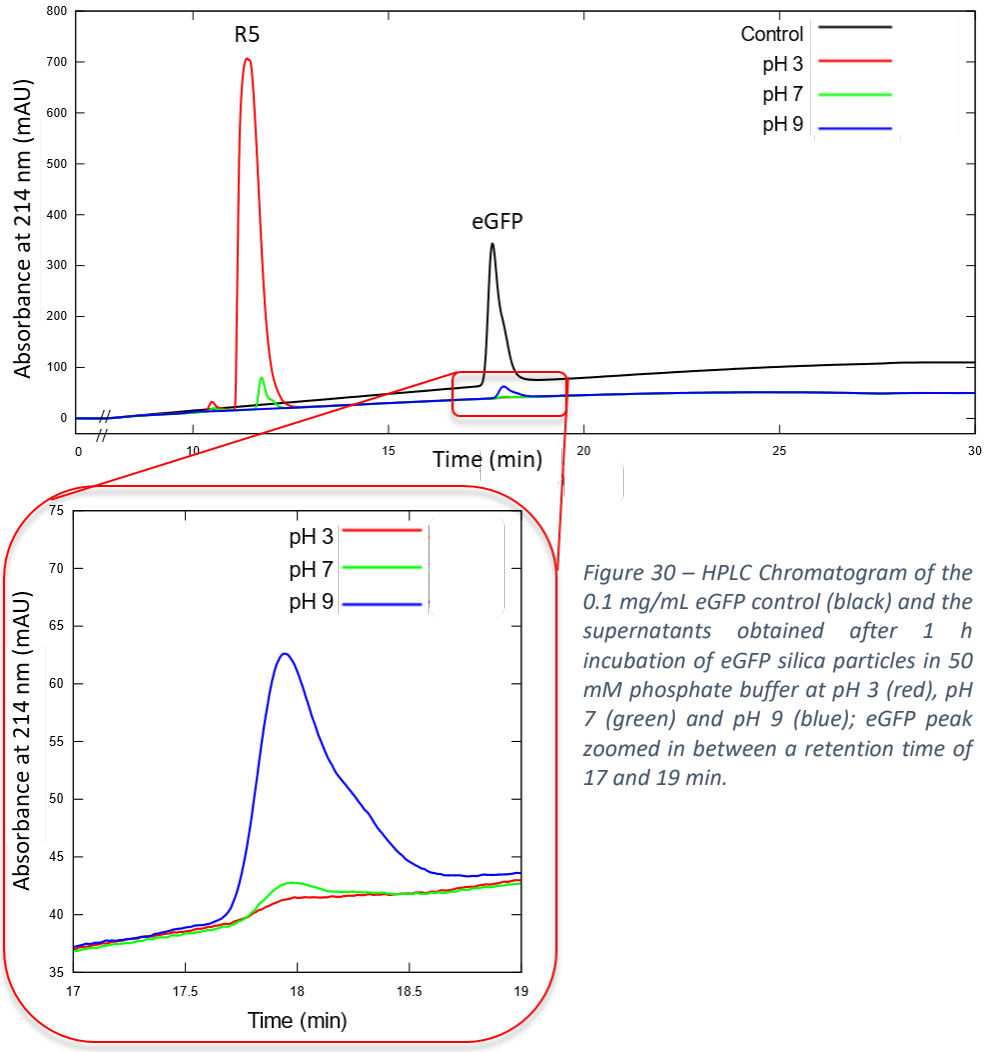

Figure 30 – HPLC Chromatogram of the 0.1 mg/mL eGFP control (black) and the supernatants obtained after 1 h incubation of eGFP silica particles in 50 mM phosphate buffer at pH 3 (red), pH 7 (green) and pH 9 (blue); eGFP peak zoomed in between a retention time of 17 and 19 min.

3.9 Protein release from Cy5-R5 silica particles

3.9.1 Release of eGFP and Cy5-R5

The release of eGFP from Cy5-R5 silica particles was determined as specified in 2.9.1. The peak area at 214 nm using pH 9 buffer is nearly halved compared to the data for the normal silica particles (Tables 20 and 21). The calculation for the 1 h approach resulted in an eGFP release of 5.63±4.30 nmol/g silica at pH 3, 2.10±0.48 nmol/g silica at pH 7 and 38.04±3.41 nmol/g silica at pH 9 (Tables 22 and 23, Figure 31A). To see if additional eGFP can be released after a longer incubation time, another trial with overnight (16 h) release was performed (Table 24). After 16 h, 2.86±0.99 nmol/g silica at pH 3, 0.94±0.44 nmol/g silica at pH 7 and 83.26±9.79 nmol/g silica at pH 9 was released (Table 25, Figure 31B). The results show that less eGFP is released using Cy5-R5 silica particles after 1 h compared to normal silica particles (54.97 ± 2.05 nmol/g silica). However, the experiment with 16 h release time proved that eGFP can be released in equal amounts but after a longer incubation time. As 272.21 ± 9.12 nmol eGFP/g silica has been adsorbed according to the results in 3.6.1, approximately 31% of eGFP was released after 16 h of incubation time.

Table 22 - Release results for eGFP using Cy5-R5 silica particles; 50 mM phosphate buffer at pH 3, pH 7 or pH 9, incubation time 1 h, 4 mg/mL silica particle concentration; Experimental area 214 nm obtained with HPLC, injection volume 80 µL; Adjusted/calculated area for 100 µL injection volume.

Sample	Experimental area 214 nm (mAU*min), V=80 µL	Average±Error (Experimental area 214 nm, V=80 µL) (mAU*min)	Calculated area 214 nm (mAU*min), V= 100 µL	Average±Error (Calculated area 214 nm, V=100 µL) (mAU*min)
Control 1	99.32	105.50±4.38	124.16	131.87±5.47
Control 2	108.15		135.19	
Control 3	109.01		136.27	
pH 3 A	1.36	0.66±0.50	1.71	0.82±0.63
pH 3 B	0.23		0.28	
pH 3 C	0.39		0.48	
pH 7 A	0.28	0.25±0.06	0.36	0.31±0.07
pH 7 B	0.29		0.36	
pH 7 C	0.17		0.21	
pH 9 A	5.02	4.46±0.40	6.27	5.57±0.50
pH 9 B	4.10		5.12	
pH 9 C	4.26		5.32	

*Table 23 – Release results for eGFP using Cy5-R5 silica particles; 50 mM phosphate buffer at pH 3, pH 7 or pH 9, incubation time 1 h, 4 mg/mL silica particle concentration; Calculated area 214 nm (mAU*min) V= 100 µL as seen in table 22 used for calculation according to equations 1 to 3.*

Sample	C [EGFP] (nmol/g silica)	Average ± Error (nmol/g silica)
pH 3 A	11.65	5.63±4.30
pH 3 B	1.93	
pH 3 C	3.30	
pH 7 A	2.43	2.10±.048
pH 7 B	2.45	
pH 7 C	1.43	
pH 9 A	42.81	38.04±3.41
pH 9 B	34.99	
pH 9 C	36.32	

Table 24 - Release results for eGFP using Cy5-R5 silica particles; 50 mM phosphate buffer at pH 3, pH 7 or pH 9, incubation time 16 h, 4 mg/mL silica particle concentration; Experimental area 214 nm obtained with HPLC, injection volume 80 µL; Adjusted/calculated area for 100 µL injection volume.

Sample	Experimental area 214 nm (mAU*min), V=80 µL	Average±Error (Experimental area 214 nm, V=80 µL) (mAU*min)	Calculated area 214 nm (mAU*min) V= 100 µL	Average±Error (Calculated area 214 nm, V=100 µL) (mAU*min)
Control 1	114.86	115.26±0.85	143.58	144.07±1.06
Control 2	116.44		145.54	
Control 3	114.47		143.09	
pH 3 A	0.19	0.37±0.13	0.23	0.46±0.16
pH 3 B	0.48		0.60	
pH 3 C	0.43		0.54	
pH 7 A	0.05	0.12±0.06	0.07	0.15±0.07
pH 7 B	0.12		0.14	
pH 7 C	0.19		0.24	
pH 9 A	9.87	10.66±1.25	12.34	13.32±1.57
pH 9 B	12.43		15.53	
pH 9 C	9.67		12.09	

*Table 25 – Release results for eGFP using Cy5-R5 silica particles; 50 mM phosphate buffer at pH 3, pH 7 or pH 9, incubation time 1 h, 4 mg/mL silica particle concentration; Calculated area 214 nm (mAU*min) V= 100 µL as seen in table 24 used for calculation according to equations 1 to 3.*

Sample	C [EGFP] (nmol/g silica)	Average ± Error (nmol/g silica)
pH 3 A	1.46	2.86±0.99
pH 3 B	3.72	
pH 3 C	3.39	
pH 7 A	0.42	0.94±0.44
pH 7 B	0.90	
pH 7 C	1.49	
pH 9 A	77.12	83.26±9.79
pH 9 B	97.07	
pH 9 C	75.59	

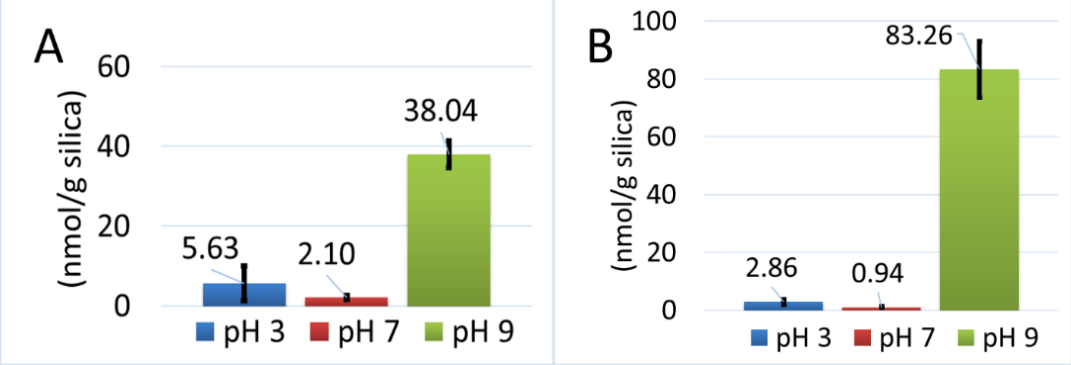

*Figure 31 – EGFP release using Cy5-R5 silica particles, **A**: Release after 1 h incubation time (refer to table 23); **B**: Release after 16 h incubation time (refer to table 25).*

The fluorescence measurement of the 1:8 diluted supernatant gave the biggest value for eGFP at pH 9 with 28,831 fluorescence counts (Figure 32A). Release of Cy5-R5 could not be quantified using HPLC measurement as it was done for eGFP due to the fact that unmodified R5 is eluting at the same time as Cy5-R5. Both substances could not be separated with the employed chromatography conditions. However, the fluorescence measurement of the supernatants showed that Cy5-R5 was released at pH 3 with 21,300 fluorescence counts (Figure 32B). Having an exact opposite pH dependent behavior, both substances could be released with retention of the other. A SEM image of the particles after eGFP release is shown in Figure 32C. Again, no significant difference which would indicate an influence of the buffer treatment is visible.

Tabelle 26 - Fluorescence counts for eGFP and Cy5-R5 release at pH 3, 7 and 9, eGFP: Emission: 509 nm, Excitation: 395 nm; Cy5: Emission: 670 nm, Excitation: 620 nm; fluorescence measurement of 1:8 diluted supernatants (V=100 µL)

Sample	Fluorescence counts pH 3	Fluorescence counts pH 7	Fluorescence counts pH 9
Sample 1 eGFP	1256	5115	30548
Sample 2 eGFP	2232	5482	28985
Sample 3 eGFP	1067	5629	26960
Average±Error	1518±511	5409±216	28831±1469
Sample 1 Cy5-R5	21323	1416	1302
Sample 2 Cy5-R5	21528	1594	1107
Sample 3 Cy5-R5	21048	1420	1102
Average±Error	21300±197	1477±83	1170±93

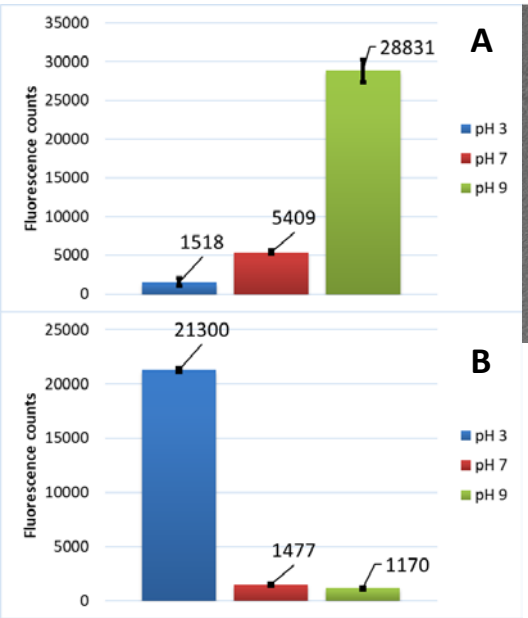

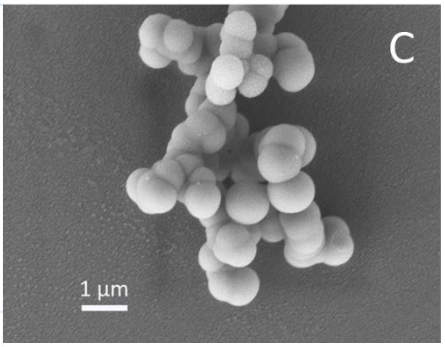

*Figure 32 – Fluorescence counts for eGFP **(A)** and Cy5-R5 **(B)** release at pH 3, 7 and 9, eGFP: Emission: 509 nm, Excitation: 395 nm; Cy5: Emission: 670 nm, Excitation: 620 nm;* fluorescence measurement of 1:8 diluted supernatants (V=100 µL) ***C**: SEM image of Cy5-R5 silica particles after treatment with 50 mM potassium phosphate buffer pH 9 for eGFP release.*

3.9.2 Release of eGFP and Cy5-R5 after ethanol drying

After Cy5-R5 silica particles were dried for 1 h using undiluted ethanol at room temperature, eGFP was released using the protocol described in 2.9.2. This was done to investigate whether eGFP is safely stored inside the silica particles even if they are not suspended in a solution. The results in Figure 33A and B show that it was still possible to release a fluorescent functional eGFP and Cy5-R5 after ethanol drying. Though no quantity measurement was performed, a dilution factor of 1:2 compared to a dilution factor of 1:8 (Figure 32) indicates, that either a lower amount of eGFP was released after ethanol drying or that most eGFP molecules were not fluorescent anymore. For Cy5-R5 the fluorescence signal is higher than fourfold signa as seen in Figure 32. The pH

dependent release behavior of both cargos remained the same as for previous experiments.

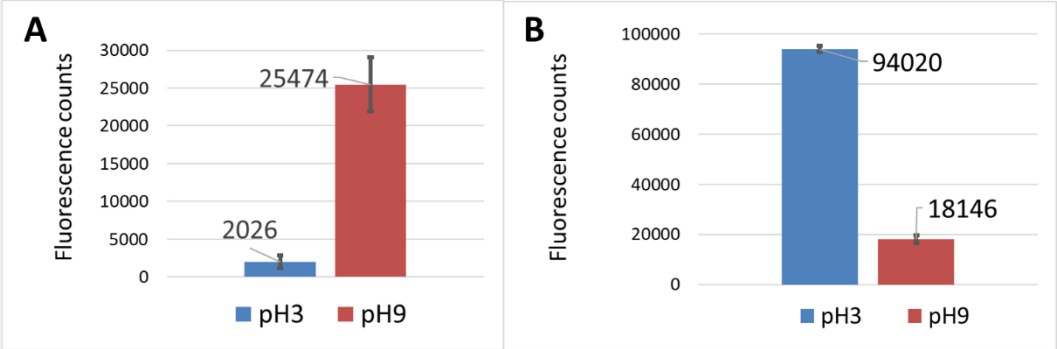

*Figure 33 – Release of eGFP and Cy5-R5 after ethanol drying using Cy5-R5 silica particles, 1:2 diluted supernatants (100µL); **A**: eGFP release Emission: 509 nm, Excitation: 395 nm; **B**: Cy5-R5 release Emission: 670 nm, Excitation: 620 nm.*

3.10 Discussion of silica and Cy5-R5 silica particles release studies

To conclude, we were able to show that both eGFP and Cy5-R5 could be released using respective silica particles. Both proteins exhibited a pH dependent release behavior where eGFP was released under basic conditions while Cy5-R5 was released using acidic conditions. However, having both cargo in one approach using Cy5-R5 silica particles, it was possible to release each cargo in retention of the other. While having a release of 22% eGFP using silica particles (1 h) and 31% eGFP using Cy5-R5 silica particles (16 h) it is of interest to increase the incubation time in order to investigate how long it takes to release the maximum amount of cargo. Although it has not been investigated why each condition led to the release of the respective cargo, the pH selective release behavior hints that it must be a pH dependent interaction such as hydrogen bonds or electrostatic interactions such as previously discussed in respect to the adsorption behavior.

A pH dependent release behavior is of great interest while developing drug carrier systems because in human body different cell compartments or different body parts exhibit different pH values. Knowing the pH dependent release behavior of a carrier molecule and material can help establish new drug/carrier systems releasing the drug agent only in specific body parts. The pH dependent release behavior of Cy5-R5 was expected since Lechner *et al.*[52] published in 2013 that they were able to release R5-Cys(SH) at pH 5 while employing 100 mM NaOAc buffer. They further concluded that R5 is not covalently bound to silica particles after precipitation but rather adsorbs onto silica through electrostatic interactions and hydrogen bonds. Having an acidic pH, the silanol groups present on the silica particle's surface and the ε-lysine amino groups of the R5 peptide are protonated. This has a negative impact on hydrogen bonds resulting in the release of the R5 peptide out of the silica particles[52]. This was also observed in our

experiments with the unmodified R5 silica particles where the R5 peptide was released at pH 3 (see Figure 30). Del Favero *et al.*[93] utilized this behavior to modify the peptide R5 with a quercetin building block. Using a 50 mM potassium phosphate buffer, they found that 45% of the quercetin-R5 was released at pH 4 after 5 h of incubation. They were further able to show that these quercetin-R5 silica particles were taken up into HT-29 cells[93]. This release behavior offers the possibility to use silica particles as drug carriers when drug release under acidic conditions is of interest e.g. in tumor tissue[94].

Xu *et al*.[95] published another pH dependent drug release system in 2011. They loaded mesoporous silica particles with ibuprofen through adsorption of the drug agent. Out of this ibuprofen loaded silica particles, a tablet was formed which was then coated using EudragitS-100. They simulated body fluids with pH 1.2 HCl (stomach) and pH 7.4 buffer (intestine) at 37 °C. They reported that ibuprofen was released at pH 7.4 but remained in the tablet at pH 1.2 due to pH sensitive coating with Eudragit[95]. Another coating substance is for example hydroxypropyl methylcellulose phthalate (HPMCP) which was used by Xu *et al*.[96] for coating of famotidine adsorbed SBA-15 tablets. An additional pH dependent release approach published by Song *et al*.[97] employed polyacrylic acid (PAA) as coating of BSA loaded SBA-15 silica particles. The particles were loaded with BSA using a citrate– phosphate buffer solution (pH 4.7) with an incubation time of 24 h. They were able to show that BSA was entrapped within the silica pores at pH 1.2 while it was released at pH 7.4. According to Song *et al*., this could possibly be due to the removal of the PAA coating at higher pH values because it swells and dissolves[97].

In our experiments, eGFP and Cy5-R5 exhibited a pH sensitive behavior without the use of a coating. However, it could be interesting to employ different coating materials to see if the pH dependent behavior can be altered thus protecting the cargo of silica particles after oral administration. Oral administration was imitated by Xu *et al*.[88] and Song *et al*.[97] by using HCl and a neutral buffer. Currently, the cargo attached to R5 in our experiments would probably be released under acidic conditions while in stomach and digested, in worst case, thus not being effective for a patient in treatment. However, Cy5-R5 was mere released at pH 7 in relatively low amounts thus not likely to be released rapidly while in intestine. This could indicate, that our approach using R5 might not be suitable for oral administration as long as the peptide conjugate is not released under basic conditions. Therefore, additional research should be performed.

However, other techniques despite oral administration for silica particles are considerable. Mohammadpour *et al.*[98] investigated the chronic toxicity of intravenously administered silica nano particles (SNPs) in mice. They found that one year after a single injection, the weight to body ratio percent of several organs were not significantly changed when comparing the control group with the mice having been treated with SNPs at their 10-day maximum tolerable dose (MTD). Additionally, various blood cells were counted such as red and white blood cells with no significant difference between both groups. However, they observed a few mice suffering from microscopic lesions in liver, kidney and spleen. Liver is already known to be the organ where silica nano particles likely accumulate after an intravenously injection. Furthermore, the utilized SNPs did not cause hemolysis in human blood samples ex vivo. They concluded that the performed injection

did not cause a statistically relevant chronic toxicity in mice because the lesions were found in the group having received injections with large, non-porous SNPs[98].

It is also possible to administer silica nano particles via subcutaneous injections. Hajizade *et al.*[99] published in 2019 that they loaded mesoporous silica nano particles (MSNPs, diameter: ~97 nm) with the recombinant EspA protein, an immunogen against enterohaemorrhagic *E. coli*. They administered this immunogen orally and subcutaneously to mice. The obtained results showed that subcutaneously administration was more efficient with respect to the immune response when compared to oral administration. The performed IL-4 assay showed the highest values of the cytokine for the immunogen loaded MSNPs and hence higher humoral immunity stimulation. They concluded that MSNPs are appropriate carriers for recombinant subunit vaccines that needs to be investigated further referring to their mechanism for immune system stimulation[99].

Chapter 4

Conclusion and outlook

To conclude, we were able to synthesize two different types of silica particles using peptides **4** and **6**. These particles were further used for protein loading experiments using eGFP and TRX as well as release experiments using eGFP and Cy5-R5 (**6**). We could show that protein was adsorbed onto silica particles and could be released again in a pH dependent approach. For eGFP and Cy5-R5 a release with retention of the other was achieved using basic (pH 9) and acidic (pH 3) conditions. Both adsorption and release of eGFP could be quantified using HPLC measurement at 214 nm. For TRX, adsorption was quantified as for eGFP but the activity measurement for the adsorbed TRX was not successful. To determine whether the enzyme is still active while adsorbed onto silica particles another method for activity measurement could be utilized which does not measure the turbidity of the solution. For this, another enzyme e.g. alcohol dehydrogenase can be trialed which could be measured with a NADP/NADPH approach. Furthermore, we could show that silica particles can act like storage reservoirs protecting a protein from outside conditions. This was done by drying of eGFP silica particles with ethanol after which a successful release of intact fluorescent eGFP and Cy5-R5 was still possible.

For future experiments, the silica particles could be loaded with other proteins e.g. supercharged GFP[100] or small drugs such as immune active molecules. It would also be interesting to attach known anticancer molecules to R5 which could then be probably released at acidic pH values as they are present inside tumor tissues. This could be also trialed in cell tests with a focus on release behavior as well as their anticancer effect.

Despite that, it would be of interest to evaluate general properties of R5 precipitated silica such as pI value, porocity and pore size. These properties could be essential to understand the kind of interactions between R5 silica and adsorbed protein in order to find out why both proteins were adsorbed at pH7 and if adsorption could be increased further employing some of the techniques found in literature which were discussed before. When silica is to be used as a drug carrier, it is of high importance to find specific conditions which favor the adsorption of the respective free drug as well as a sustained release of the drug agent in order to be effective for patients in treatment. Additionally, the administration technique and both its advantages and disadvantages needs to be determined when using silica particles as drug or vaccine carriers.

References

[1] C. Y. Wong, H. Al-Salami, C. R. Dass, *Int. J. Pharm.* **2018**, *549*, 201–217.
[2] Verma et al., *Int. J. Pharm. Stud. Res.* **2010**, *Vol. I*, 54–59.
[3] M. Gibaldi, R. N. Boyes, S. Feldman, *J. Pharm. Sci.* **1971**, *60*, 1338–1340.
[4] N. Gulati, H. Gupta, *Recent Pat. Drug Deliv. Formul.* **2011**, *5*, 133–145.
[5] T. M. Allen, *Science* **2004**, *303*, 1818–1822.
[6] H. Daraee, A. Etemadi, M. Kouhi, S. Alimirzalu, A. Akbarzadeh, *Artif. Cells Nanomedicine Biotechnol.* **2016**, *44*, 381–391.
[7] E. M. Bolotin, R. Cohen, L. K. Bar, N. Emanuel, S. Ninio, Y. Barenholz, D. D. Lasic, *J. Liposome Res.* **1994**, *4*, 455–479.
[8] J. M. Harris, N. E. Martin, M. Modi, *Clin. Pharmacokinet.* **2001**, *40*, 539–551.
[9] J. Huwyler, D. Wu, W. M. Pardridge, *Proc. Natl. Acad. Sci.* **1996**, *93*, 14164–14169.
[10] P. L. Felgner, T. R. Gadek, M. Holm, R. Roman, H. W. Chan, M. Wenz, J. P. Northrop, G. M. Ringold, M. Danielsen, *Proc. Natl. Acad. Sci.* **1987**, *84*, 7413–7417.
[11] Y. Inoh, M. Nagai, K. Matsushita, M. Nakanishi, T. Furuno, *Eur. J. Pharm. Sci.* **2017**, *102*, 230–236.
[12] C. R. Alving, *J. Immunol. Methods* **1991**, *140*, 1–13.
[13] H. S. Oberoi, Y. M. Yorgensen, A. Morasse, J. T. Evans, D. J. Burkhart, *J. Controlled Release* **2016**, *223*, 64–74.
[14] A. Akbarzadeh, R. Rezaei-Sadabady, S. Davaran, S. W. Joo, N. Zarghami, Y. Hanifehpour, M. Samiei, M. Kouhi, K. Nejati-Koshki, *Nanoscale Res. Lett.* **2013**, *8*, 102.
[15] H. Takeuchi, H. Yamamoto, T. Toyoda, H. Toyobuku, T. Hino, Y. Kawashima, *Int. J. Pharm.* **1998**, *164*, 103–111.
[16] C. Bern, J. Adler-Moore, J. Berenguer, M. Boelaert, M. den Boer, R. N. Davidson, C. Figueras, L. Gradoni, D. A. Kafetzis, K. Ritmeijer, E. Rosenthal, C. Royce, R. Russo, S. Sundar, J. Alvar, *Clin. Infect. Dis.* **2006**, *43*, 917–924.
[17] D. da-Silva-Freitas, J. Boldrini-França, E. Arantes, *Protein Pept. Lett.* **2015**, *22*, 1133–1139.
[18] P. Milla, F. Dosio, L. Cattel, *Curr. Drug Metab.* **2012**, *13*, 105–119.
[19] H. Hatakeyama, H. Akita, H. Harashima, *Biol. Pharm. Bull.* **2013**, *36*, 892–899.
[20] J. W. Nichols, Y. H. Bae, *J. Controlled Release* **2014**, *190*, 451–464.
[21] Y. Matsumura, H. Maeda, *Cancer Res.* **1986**, *46*, 6387–6392.
[22] J.-H. Kao, C.-H. Liu, *Int. J. Nanomedicine* **2014**, 2051.
[23] J. Thomas, H. Levy, S. Amato, J. Vockley, R. Zori, D. Dimmock, C. O. Harding, D. A. Bilder, H. H. Weng, J. Olbertz, M. Merilainen, J. Jiang, K. Larimore, S. Gupta, Z. Gu, H. Northrup, *Mol. Genet. Metab.* **2018**, *124*, 27–38.
[24] P. A. Dinndorf, J. Gootenberg, M. H. Cohen, P. Keegan, R. Pazdur, *The Oncologist* **2007**, *12*, 991–998.
[25] P. P. Wibroe, D. Ahmadvand, M. A. Oghabian, A. Yaghmur, S. M. Moghimi, *J. Controlled Release* **2016**, *221*, 1–8.
[26] T. Ishii, T. Asai, D. Oyama, T. Fukuta, N. Yasuda, K. Shimizu, T. Minamino, N. Oku, *J. Controlled Release* **2012**, *160*, 81–87.
[27] B. Sun, M. Zhang, J. Shen, Z. He, P. Fatehi, Y. Ni, *Curr. Med. Chem.* **2019**, *26*, 2485–2501.

[28] Ankita Raizada et al., *Int. J. Pharma Res. Dev.* **2010**, *2*, 9–20.
[29] J. Pushpamalar, A. K. Veeramachineni, C. Owh, X. J. Loh, *ChemPlusChem* **2016**, *81*, 504–514.
[30] S. Freiberg, X. X. Zhu, *Int. J. Pharm.* **2004**, *282*, 1–18.
[31] K. Pal, B. Behera, S. Roy, S. Sekhar Ray, G. Thakur, *Soft Mater.* **2013**, *11*, 125–142.
[32] W. Stöber, A. Fink, E. Bohn, *J. Colloid Interface Sci.* **1968**, *26*, 62–69.
[33] L. L. Hench, J. K. West, *Chem. Rev.* **1990**, *90*, 33–72.
[34] I. A. Rahman, V. Padavettan, *J. Nanomater.* **2012**, *2012*, 1–15.
[35] G. Grün et al. et al., *Adv Mater Adv. Mater. Weinh.* **1997**, *9*, 254–257.
[36] R. Narayan, U. Nayak, A. Raichur, S. Garg, *Pharmaceutics* **2018**, *10*, 118.
[37] I. Slowing, J. Viveroescoto, C. Wu, V. Lin, *Adv. Drug Deliv. Rev.* **2008**, *60*, 1278–1288.
[38] J. Xu, Z. Luan, H. He, W. Zhou, L. Kevan, *Chem. Mater.* **1998**, *10*, 3690–3698.
[39] L. Wei, N. Hu, Y. Zhang, *Materials* **2010**, *3*, 4066–4079.
[40] C. Bharti, N. Gulati, U. Nagaich, A. Pal, *Int. J. Pharm. Investig.* **2015**, *5*, 124.
[41] S. Shi, F. Chen, W. Cai, *Nanomed.* **2013**, *8*, 2027–2039.
[42] X. She, L. Chen, C. Li, C. He, L. He, L. Kong, *J. Nanomater.* **2015**, *2015*, 1–9.
[43] K.-C. Kao, C.-Y. Mou, *Microporous Mesoporous Mater.* **2013**, *169*, 7–15.
[44] Y. Wang, Y. Sun, J. Wang, Y. Yang, Y. Li, Y. Yuan, C. Liu, *ACS Appl. Mater. Interfaces* **2016**, *8*, 17166–17175.
[45] S.-H. Cheng, C.-H. Lee, M.-C. Chen, J. S. Souris, F.-G. Tseng, C.-S. Yang, C.-Y. Mou, C.-T. Chen, L.-W. Lo, *J. Mater. Chem.* **2010**, *20*, 6149.
[46] K. Cheng, Y. Zhang, Y. Li, Z. Gao, F. Chen, K. Sun, P. An, C. Sun, Y. Jiang, B. Sun, *J. Mater. Chem. B* **2019**, *7*, 3291–3302.
[47] S. Sapino, E. Ugazio, L. Gastaldi, I. Miletto, G. Berlier, D. Zonari, S. Oliaro-Bosso, *Eur. J. Pharm. Biopharm.* **2015**, *89*, 116–125.
[48] M. Sumper, E. Brunner, *Adv. Funct. Mater.* **2006**, *16*, 17–26.
[49] V. Martin-Jezequel, M. Hildebrand, M. A. Brzezinski, *J. Phycol.* **2000**, *36*, 821–840.
[50] M. Hildebrand, B. E. Volcani, W. Gassmann, J. I. Schroeder, *Nature* **1997**, *385*, 688–689.
[51] T. L. Simpson, B. E. Volcani, *Silicon and Siliceous Structures in Biological Systems*, Springer-Verlag, New York, NY, **2011**.
[52] C. Lechner, Functional Analysis and Biotechnological Applications of Silaffin Peptides, **2013**.
[53] C. Exley, *J. Inorg. Biochem.* **1998**, *69*, 139–144.
[54] N. Kröger, N. Poulsen, *Annu. Rev. Genet.* **2008**, *42*, 83–107.
[55] *J. Mar. Biol. Assoc. U. K.* **1990**, *70*, 924–924.
[56] N. Kröger, *Science* **1999**, *286*, 1129–1132.
[57] N. Kröger, R. Deutzmann, M. Sumper, *J. Biol. Chem.* **2001**, *276*, 26066–26070.
[58] N. Kröger, S. Lorenz, E. Brunner, M. Sumper, *Science* **2002**, *298*, 584–586.
[59] T. Mizutani, H. Nagase, N. Fujiwara, H. Ogoshi, *Bull. Chem. Soc. Jpn.* **1998**, *71*, 2017–2022.
[60] E. Baeuerlein, Ed. , *Biomineralization: Progress in Biology, Molecular Biology and Application*, Wiley-VCH, Weinheim, **2004**.
[61] C. C. Lechner, C. F. W. Becker, *J. Pept. Sci.* **2014**, *20*, 152–158.
[62] C. C. Lechner, C. F. W. Becker, *Chem. Sci.* **2012**, *3*, 3500.
[63] E. L. Buckle, J. Sampath, N. Michael, S. D. Whedon, C. J. A. Leonen, J. Pfaendtner, G. P. Drobny, C. Chatterjee, *ChemBioChem* **2020**, cbic.202000264.
[64] C. C. Lechner, C. F. W. Becker, *Biomater. Sci.* **2015**, *3*, 288–297.

[65] J. S. Edwards, A. Kumbhar, A. Roberts, A. C. Hemmert, C. C. Edwards, P. M. Potter, M. R. Redinbo, *Biotechnol. Prog.* **2011**, *27*, 863–869.
[66] Birgit Bräuer, Biomimetic Synthesis of Multifunctional Silica Particles, **2017**.
[67] O. Shimomura, F. H. Johnson, Y. Saiga, *J. Cell. Comp. Physiol.* **1962**, *59*, 223–239.
[68] F. G. Prendergast, K. G. Mann, *Biochemistry* **1978**, *17*, 3448–3453.
[69] M. Chalfie, Y. Tu, G. Euskirchen, W. Ward, D. Prasher, *Science* **1994**, *263*, 802–805.
[70] D. C. Prasher, V. K. Eckenrode, W. W. Ward, F. G. Prendergast, M. J. Cormier, *Gene* **1992**, *111*, 229–233.
[71] R. Y. Tsien, *Annu. Rev. Biochem.* **1998**, *67*, 509–544.
[72] O. Shimomura, *FEBS Lett.* **1979**, *104*, 220–222.
[73] C. W. Cody, D. C. Prasher, W. M. Westler, F. G. Prendergast, W. W. Ward, *Biochemistry* **1993**, *32*, 1212–1218.
[74] M. Zimmer, *Chem. Rev.* **2002**, *102*, 759–782.
[75] M. Z. Pozzan Tullio, *IUBMB Life Int. Union Biochem. Mol. Biol. Life* **2000**, *49*, 375–379.
[76] J. Born, F. Pfeifer, *Front. Microbiol.* **2019**, *10*, 1200.
[77] T. C. Laurent, E. C. Moore, P. Reichard, *J. Biol. Chem.* **1964**, *239*, 3436–3444.
[78] A. Holmgren, *Annu. Rev. Biochem.* **1985**, *54*, 237–271.
[79] E. S. J. Arnér, A. Holmgren, *Eur. J. Biochem.* **2000**, *267*, 6102–6109.
[80] F. Sanger, *Biochem. J.* **1949**, *44*, 126–128.
[81] M. Kamalov, A. Hajradini, C. Rentenberger, C. F. W. Becker, *Mater. Lett.* **2018**, *212*, 114–117.
[82] N. Kroger, *Science* **2002**, *298*, 584–586.
[83] D. M. Schlipf, S. E. Rankin, B. L. Knutson, *ACS Appl. Mater. Interfaces* **2013**, *5*, 10111–10117.
[84] J. Tu, A. L. Boyle, H. Friedrich, P. H. H. Bomans, J. Bussmann, N. A. J. M. Sommerdijk, W. Jiskoot, A. Kros, *ACS Appl. Mater. Interfaces* **2016**, *8*, 32211–32219.
[85] D. Zhao, *Science* **1998**, *279*, 548–552.
[86] D. Zhao, J. Sun, Q. Li, G. D. Stucky, *Chem. Mater.* **2000**, *12*, 275–279.
[87] M. Mesa, L. Sierra, B. López, A. Ramirez, J.-L. Guth, *Solid State Sci.* **2003**, *5*, 1303–1308.
[88] K. Kubiak-Ossowska, B. Jachimska, P. A. Mulheran, *J. Phys. Chem. B* **2016**, *120*, 10463–10468.
[89] K. Kubiak-Ossowska, K. Tokarczyk, B. Jachimska, P. A. Mulheran, *J. Phys. Chem. B* **2017**, *121*, 3975–3986.
[90] U. Umakoshi et al., **2009**, *16*, 145–150.
[91] J. Meissner, A. Prause, B. Bharti, G. H. Findenegg, *Colloid Polym. Sci.* **2015**, *293*, 3381–3391.
[92] Y. Ma, P. Rajendran, C. Blum, Y. Cesa, N. Gartmann, D. Brühwiler, V. Subramaniam, *J. Colloid Interface Sci.* **2011**, *356*, 123–130.
[93] G. Del Favero, F. Bialas, S. Grabher, A. Wittig, B. Bräuer, D. Gerthsen, C. Echalier, M. Kamalov, D. Marko, C. F. W. Becker, *Chem. Commun.* **2019**, *55*, 9649–9652.
[94] K. H. Min, J.-H. Kim, S. M. Bae, H. Shin, M. S. Kim, S. Park, H. Lee, R.-W. Park, I.-S. Kim, K. Kim, I. C. Kwon, S. Y. Jeong, D. S. Lee, *J. Controlled Release* **2010**, *144*, 259–266.
[95] Y. Xu, F. Qu, Y. Wang, H. Lin, X. Wu, Y. Jin, *Solid State Sci.* **2011**, *13*, 641–646.
[96] W. Xu, Q. Gao, Y. Xu, D. Wu, Y. Sun, *Mater. Res. Bull.* **2009**, *44*, 606–612.
[97] S.-W. Song, K. Hidajat, S. Kawi, *Chem. Commun.* **2007**, 4396.

[98] R. Mohammadpour, D. L. Cheney, J. W. Grunberger, M. Yazdimamaghani, J. Jedrzkiewicz, K. J. Isaacson, M. A. Dobrovolskaia, H. Ghandehari, *J. Controlled Release* **2020**, *324*, 471–481.
[99] A. Hajizade, A. H. Salmanian, J. Amani, F. Ebrahimi, A. Arpanaei, *Artif. Cells Nanomedicine Biotechnol.* **2018**, *46*, S1067–S1075.
[100] B. S. Der, C. Kluwe, A. E. Miklos, R. Jacak, S. Lyskov, J. J. Gray, G. Georgiou, A. D. Ellington, B. Kuhlman, *PLoS ONE* **2013**, *8*, e64363.